Beyond the Bid–Ask: Strategic Insights into Spread Prediction and the Global Mid-Price Phenomenon

Yifan He*[1], Abootaleb Shirvani[2], Barret Shao[3], Svetlozar Rachev[1], and Frank Fabozzi[4]

[1]*Department of Mathematics and Statistics, Texas Tech University, Lubbock, TX 79409, USA*
[2]*Department of Mathematical Sciences, Kean University, Union, NJ 07083, USA*
[3]*XBTO Group, New York, NY 10019, USA*
[4]*Carey Business School, Johns Hopkins University, Baltimore, MD 21202, USA*

April 19, 2024

Abstract

This study introduces novel concepts in the analysis of limit order books (LOBs) with a focus on unveiling strategic insights into spread prediction and understanding the global mid-price (GMP) phenomenon. We define and analyze the total market order book bid–ask spread (TMOBBAS) and GMP, showcasing their significance in providing a deeper understanding of market dynamics beyond traditional LOB models. Employing high-frequency data, we comprehensively examine these concepts through various methodological lenses, including tail behavior analysis, dynamics of log-returns, and risk–return performance evaluation. Our findings reveal the intricate behavior of TMOBBAS and GMP under different market conditions, offering new perspectives on the liquidity, volatility, and efficiency of markets. This paper not only contributes to the academic discourse on financial markets but also presents practical implications for traders, risk managers, and policymakers seeking to navigate the complexities of modern financial systems.

Keywords: Limit order book; bid–ask spread; mid-price; option pricing; implied volatility; Rachev ratio

1 Introduction

The intricacies of financial markets, particularly the mechanisms underlying the formation of prices and the dynamics of spreads, have long fascinated researchers and practitioners alike. At the heart of these mechanisms lies the limit order book (LOB), a pivotal structure that records the buy and sell orders for a specific asset at different price levels. Traditionally, studies of LOBs have concentrated on understanding the bid–ask spread and mid-price dynamics, offering critical insights into the liquidity and efficiency of the markets. However, with the advent of high-frequency trading (HFT), along with the increasing complexity of financial markets, there is a need to take a closer examination of these dynamics and identify the strategies that govern spread prediction and the global mid-price (GMP) phenomenon.

Recent surveys, such as those compiled in (Gould et al., 2013), provide a comprehensive review of the empirical and theoretical advancements in our understanding of LOBs. These reviews have been instrumental in shaping current methodologies and highlighting areas where further inquiry is required, particularly in the context of high-frequency data and modern trading algorithms.

*Correspondence: `Yifan.He@ttu.edu`

In this context, we introduce two novel concepts: the total market order book bid–ask spread (TMOBBAS) and the GMP. These concepts extend beyond the traditional bid–ask spread and mid-price measures by considering the entire depth of the LOB, thereby providing a more holistic view of the market dynamics. Our study is grounded in the rich academic lineage of LOB research, drawing upon foundational work such as (Abergel et al., 2016) offering a comprehensive overview of LOB structures and their implications for market analysis. Furthermore, our exploration of TMOBBAS and GMP is informed by the theoretical underpinnings of market microstructure theory, as discussed in (O'Hara, 1998), and the empirical findings on the impact of HFT on the liquidity and volatility of a market, as in (Brogaard et al., 2014).

The introduction of TMOBBAS and GMP allows us to explore new dimensions of market behavior, particularly in relation to liquidity and volatility. By employing high-frequency data from prominent market instruments, we undertake a meticulous analysis of these concepts through various lenses, including tail behavior analysis, dynamics of log-returns, and risk–return performance evaluation. Our methodology is informed by a blend of theoretical insights and empirical analyses, ensuring a robust examination of the phenomena under study. The work of (Cont, 2001) on the empirical properties of asset returns and the stylized facts of financial markets provides a foundational basis for our analysis, while the methodologies for the tail behavior analysis draw on the advanced statistical techniques described by (McNeil et al., 2015).

The rest of this paper is organized as follows, Section 2 lays the groundwork with a discussion on LOBs and introduces the foundational concepts of TMOBBAS and GMP. Section 3 describes in detail the high-frequency data used for the analysis. Then Section 4 examines the tail behavior of the financial returns. The dynamics of log-returns are examined in Section 5 through advanced statistical models. Option pricing and implied volatility analyses for TMOBBAS and GMP are presented in Section 6. Section 7 evaluates the risk–return performance of these indices, employing the Rachev ratio for the evaluation. Section 8 presents a summary of our findings, their implications, and directions for future research.

2 Preliminaries

From (Abergel et al., 2016), we know that a LOB is essentially a file in a computer that contains all orders sent to the market, with their characteristics, such as the sign of the order, its price, quantity, and a timestamp. In academia, the usual approach involves simplifying the structure of the LOB to facilitate applying it more efficiently. Figure 1 is an example of an LOB with a simplified structure.

In Figure 1, the blue side depicts the bid prices (5, 6 and 7), representing the prices of limit buy orders, while the red side depicts the ask prices (10, 11 and 12), namely, the prices of the limit sell orders. In the bid prices and ask prices, we also encounter the corresponding best bid price and best ask price. The best bid price is the highest among the limit buy orders, while the best ask price is the lowest among the limit sell orders. Hence, in this example, the best bid price is 7 and the best ask price is 10.

When discussing the best bid price and best ask price, there are two concepts we cannot ignore. One is the bid–ask spread (BAS), the other is the mid-price. The BAS is defined as the difference between between the best ask price and the best bid price, while the mid-price is defined as the average of the bid price and the ask price. In the example in Figure 1, the BAS is $10 - 7 = 3$ and the mid-price is $(10 + 7)/2 = 8.5$.

In this paper, we define two new concepts, which contain the BAS and mid-price as special cases. Before delving into these new concepts, let us introduce a new definition:

Definition 1. (TMOBAP and TMOBBP). The *total market order book ask price* (TMOBAP) is the quotient of the value of a market order that is sufficient to purchase the entire volume of shares in the

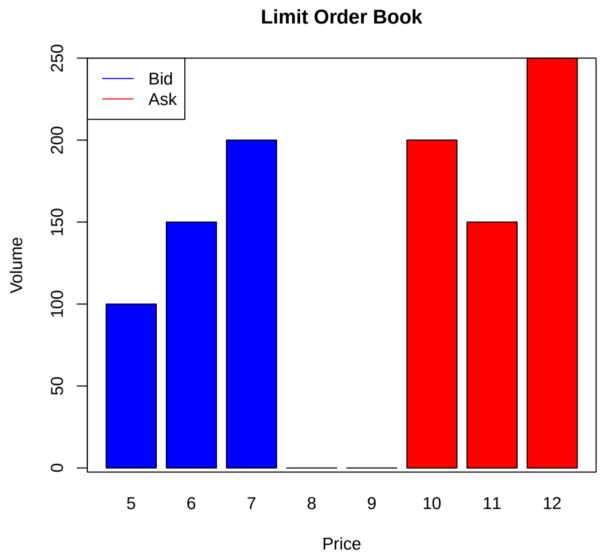

Figure 1: Example of an LOB with a simplified structure

ask limit order book by the total number of shares available in the ask limit order book. Similarly, the *total market order book bid price* (TMOBBP) is the quotient of the value of the market order that is sufficient to purchase the entire volume of shares in the bid limit order book by the total number of shares available in the bid limit order book.

Referring to Definition 1, the two new concepts we define are referred to as the *total market order book bid–ask spread* (TMOBBAS) and the *global mid-price* (GMP), respectively. They are defined as follows:

$$\text{TMOBBAS} := \text{TMOBAP - TMOBBP}, \tag{1}$$
$$\text{GMP} := (\text{TMOBAP} + \text{TMOBBP})/2. \tag{2}$$

Let us continue to use Figure 1 to provide a clearer explanation of these new terms. Based on Definition 1, Equations (1) and (2), and referencing Figure 1, we can derive the following:

$$\begin{aligned} \text{TMOBAP} &= \frac{10 \times 200 + 11 \times 150 + 12 \times 250}{200 + 150 + 250} \approx 11.08, \\ \text{TMOBBP} &= \frac{5 \times 100 + 6 \times 150 + 7 \times 200}{100 + 150 + 200} \approx 6.22, \\ \text{TMOBBAS} &:= \text{TMOBAP - TMOBBP} \approx 4.86, \\ \text{GMP} &:= (\text{TMOBAP} + \text{TMOBBP})/2 \approx 8.65. \end{aligned} \tag{3}$$

As observed, it is evident that both TMOBBAS and GMP are functions of the LOB's depth. The results in Equations (3) give TMOBBAS and GMP a depth of 3. The reason we say that BAS and mid-price are a special case of TMOBBAS and GMP, respectively, is that BAS and mid-price are actually the TMOBBAS and GMP with a depth of 1, which is easy to verify.

3 The Data

Obtaining the high-frequency LOB data with which to compute the TMOBBAS and GMP for real-world analysis is a challenging endeavor due to the value and sensitivity of this information.

Fortunately, Limit Order Book System - The Efficient Reconstructor (LOBSTER)[1] provided us with free high-frequency data samples with which to do academic research.

In our analysis, we adhere to the guidelines outlined in (Huang and Polak, 2011) to select HFT data samples for Amazon (AMZN), Apple (AAPL) and Google (GOOG) from 9:30:00 AM to 4:00:00 PM on June 21, 2012. In order to eliminate the impact of the previous trading day, we remove the first 5% of the timestamps and the corresponding data in the original data set to obtain the new dataset for us to analyze. Table 1 summarizes the dataset that we will use.

Ticker	Number of Timestamps	Maximum Value of Depth
AMZN	248,202	10
AAPL	365,113	10
GOOG	132,411	10

Table 1: Summary of our datasets

To analyze TMOBBAS or GMP at different depths, we must truncate our dataset to include a specific number of ask prices, bid prices, ask volumes and bid volumes. For instance, if we intend to examine TMOBBAS and GMP of AAPL at a depth of 2, we should truncate the dataset for AAPL to include two ask prices, two bid prices, two ask volumes and two bid volumes. Table 2 is the part of the dataset for AAPL. It is evident that to explore TMOBBAS and GMP at a depth of 2, we need to truncate nine columns, including the timestamp, two ask prices, two ask volumes (sizes), two bid prices, and two bid volumes.

Time	Ask price 1	Ask size 1	Bid price 1	Bid size 1	Ask price 2	Ask size 2	Bid price 2	Bid size 2
⋮	⋮	⋮	⋮	⋮	⋮	⋮	⋮	⋮
35159.318815640	5865700	100	5863100	100	5866100	1900	5862900	100
35159.428838154	5865700	100	5863100	100	5865900	200	5862900	100
35159.432266639	5865700	100	5863100	100	5865900	200	5862900	100
35159.439130585	5865700	100	5863200	100	5865900	200	5863100	100
35159.450166122	5865700	100	5863200	100	5865900	200	5863100	100
⋮	⋮	⋮	⋮	⋮	⋮	⋮	⋮	⋮
57599.913117637	5776700	300	5775400	410	5776800	200	5775300	1400

Table 2: Part of dataset for AAPL at depth 2

The values in the "Time" column are the time difference between the current time and midnight in seconds. For example, "34200" means 34,200 seconds from midnight, which, when converted to hours, is 9.5 hours, namely, 9:30:00 AM. Similarly, "57600" indicates 57,600 seconds from midnight, corresponding to 16 hours or 4:00:00 PM.

Regarding the price columns, "Ask price 1" is the best ask price, i.e., the lowest ask price, while "Ask price 2" is the second-best ask price. Similarly, "Bid price 1" is the best bid price, i.e., the highest bid price, and "Bid price 2" is the second-best bid price. The values in the price columns are in US dollars (USD) multiplied by 10,000. For example, "5865700" is 586.57 USD.

Lastly, the values in the size columns are the corresponding number of shares for the given ask price or bid price.

[1] The official website of LOBSTER is `https://lobsterdata.com/`.

4 Tail Behavior Analysis

4.1 Non-Gaussianity of Log-Return

Let $S_{t,d}$ denote TMOBBAS or GMP at timestamp t with a depth of d, where $34,200 \text{ s} \leq t \leq 57,600 \text{ s}$ and $1 \leq d \leq 10$. If we regard $S_{t,d}$ as the price of a specific "asset" and we are interested in exploring the return of this asset, then we can define the *log-return* $r_{t,d}$ as the following:

$$r_{t,d} := \log\left(\frac{S_{t+\Delta t,d}}{S_{t,d}}\right)$$

where $t + \Delta t$ ($\Delta t > 0$) is the timestamp for the next time step after timestamp t. The rationale for employing log-returns in this paper is grounded in the consideration that in HFT, the Δt should be very small, requiring our study to be based on a continuous-time framework. Furthermore, in a later section, we will formulate a continuous-time option pricing model, and (Shreve, 2004) emphasizes that continuous-time option pricing typically employs log-returns.

Figure 2 displays the evolution of TMOBBAS, GMP and their log-returns over time at all ten different depths for AAPL[2]. To enhance our understanding of the log-returns at various depths, we aim to examine their distributions. From Figure 3, we can directly observe that the distributions of the log-returns of TMOBBAS and GMP are decidedly non-Gaussian.

Moreover, in order to quantitatively illustrate the non-Gaussianity of the log-returns, we can compute the excess kurtosis of the log-returns. Suppose we have an independently and identically distributed (i.i.d.) sample of X with a size of n, where $\mathbb{E}(X) = \mu$ and $\mathbf{Var}(X) = \sigma^2$. Then the formula to compute the excess kurtosis is

$$\text{excess kurtosis} := \frac{\mathbb{E}[(X-\mu)^4]}{\sigma^4} - 3. \tag{4}$$

The reason for subtracting 3 in Equation (4) is to make sure the excess kurtosis of the Gaussian distribution is zero. In addition to the traditional excess kurtosis, we also propose a robust measure of excess kurtosis in detecting a distribution's tails, as suggested by (Hogg, 1972, 1974):

$$\text{robust excess kurtosis} := \frac{U_{0.05} - L_{0.05}}{U_{0.5} - L_{0.5}} - 2.59, \tag{5}$$

where $U_\alpha := \frac{1}{\alpha}\int_{1-\alpha}^{1} F^{-1}(y)\,\mathrm{d}y$, $L_\alpha := \frac{1}{\alpha}\int_{0}^{\alpha} F^{-1}(y)\,\mathrm{d}y$ and $F^{-1}(y)$ is the y-th quantile of the sample distribution. Still, the reason for subtracting 2.59 in Equation (5) is to ensure that the robust excess kurtosis of the Gaussian distribution is zero.

Figure 4 displays the evolution of the log-returns of TMOBBAS and GMP over depths for AMZN, AAPL, and GOOG. From Figure 4, we can observe that both the excess kurtosis and the robust excess kurtosis for each depth are significantly greater than zero, indicating that the distribution of the log-returns of TMOBBAS and GMP for these three stocks is *leptokurtic*.

In summary, to capture the entire density of the log-returns for TMOBBAS and GMP, we need to take into account a non-Gaussian distribution that has tails that asymptotically approach zero more slowly than a Gaussian distribution. From previous work ((Rachev and Mittnik, 2000), (Cont, 2001), (Shimokawa et al., 2007), (Lux, 2009), (Rogers and Zhang, 2011), *etc.* among others), we know that when facing such a problem, we typically examine the tail behavior first to determine the nature of the distribution's tail. Moreover, tail estimation allows us to gain insights directly from

[2]To conserve space, our primary focus in the main text will be on AAPL from this section on, due to its having the largest market capitalization up to 2024 among these three stocks. Comparable analyses for AMZN and GOOG can be found in Appendix A and Appendix B, respectively. Since the analyses for AMZN and GOOG are similar to that for AAPL, we will only provide related graphs but ignore the explanatory text.

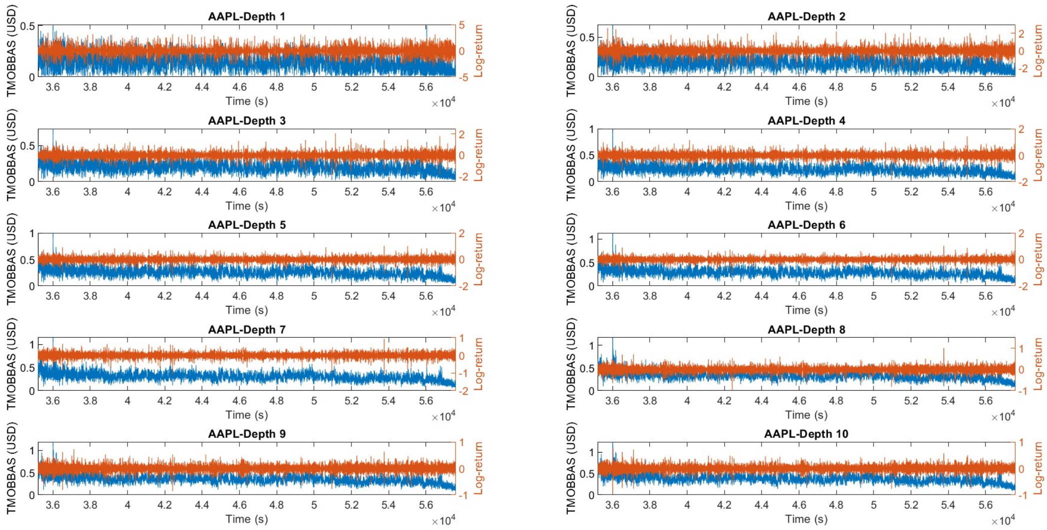

(a)

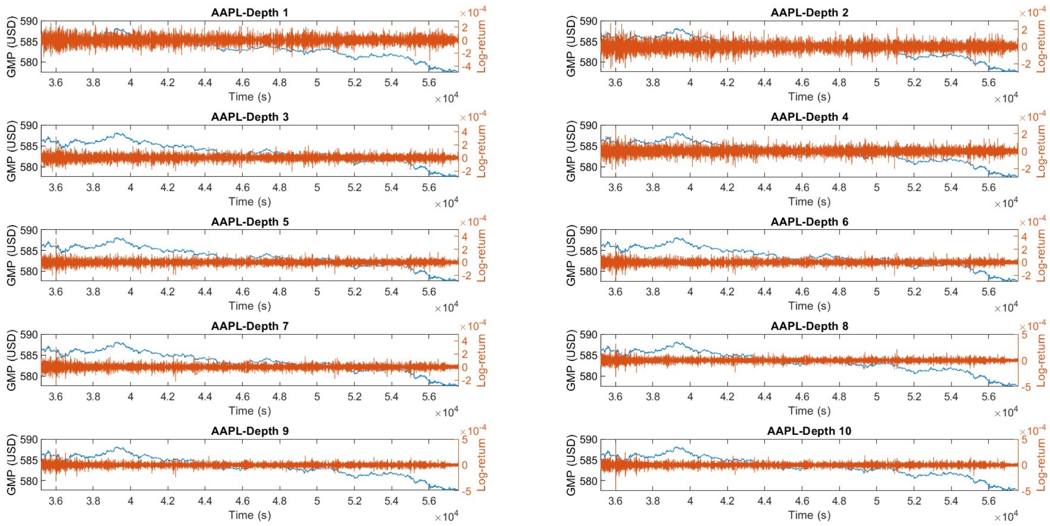

(b)

Figure 2: The evolution of (a) TMOBBAS, (b) GMP and their log-return over time at all 10 different depths for AAPL (Each graph contains two y-axes. The left y-axis indicates the size of TMOBBAS or GMP, and the right y-axis indicates the size of log-return. The evolution of TMOBBAS or GMP is represented by the blue line while the evolution of the log-return is denoted by the orange line.)

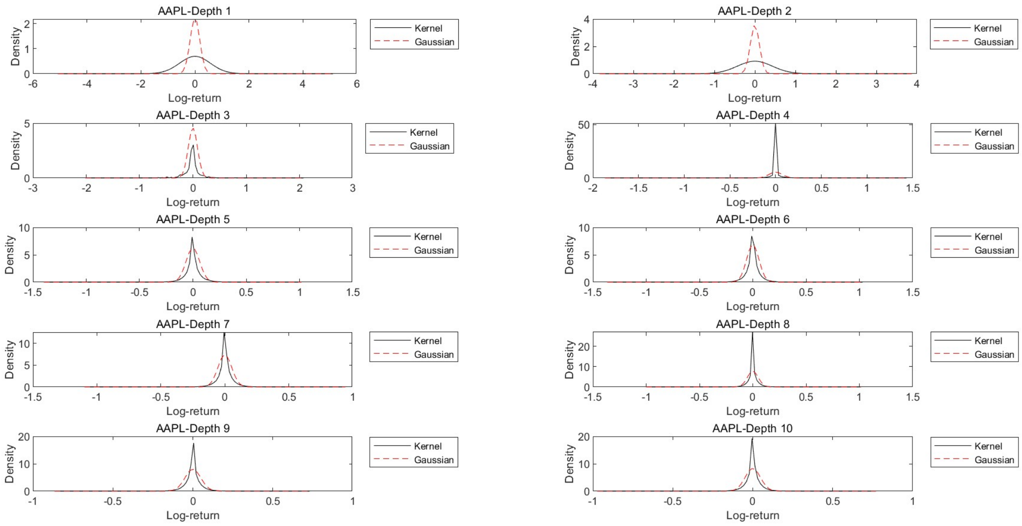

(a)

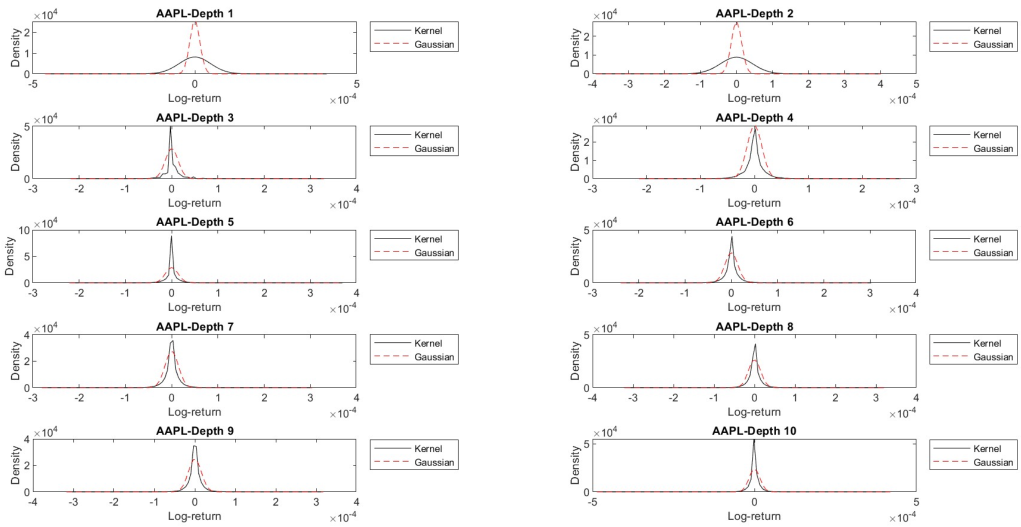

(b)

Figure 3: Comparison between the kernel density (represented by black solid lines) of log-returns of (a) TMOBBAS, (b) GMP and the corresponding Gaussian distribution with the same sample mean and standard deviation (depicted by the red dashed lines) at all 10 depths for AAPL

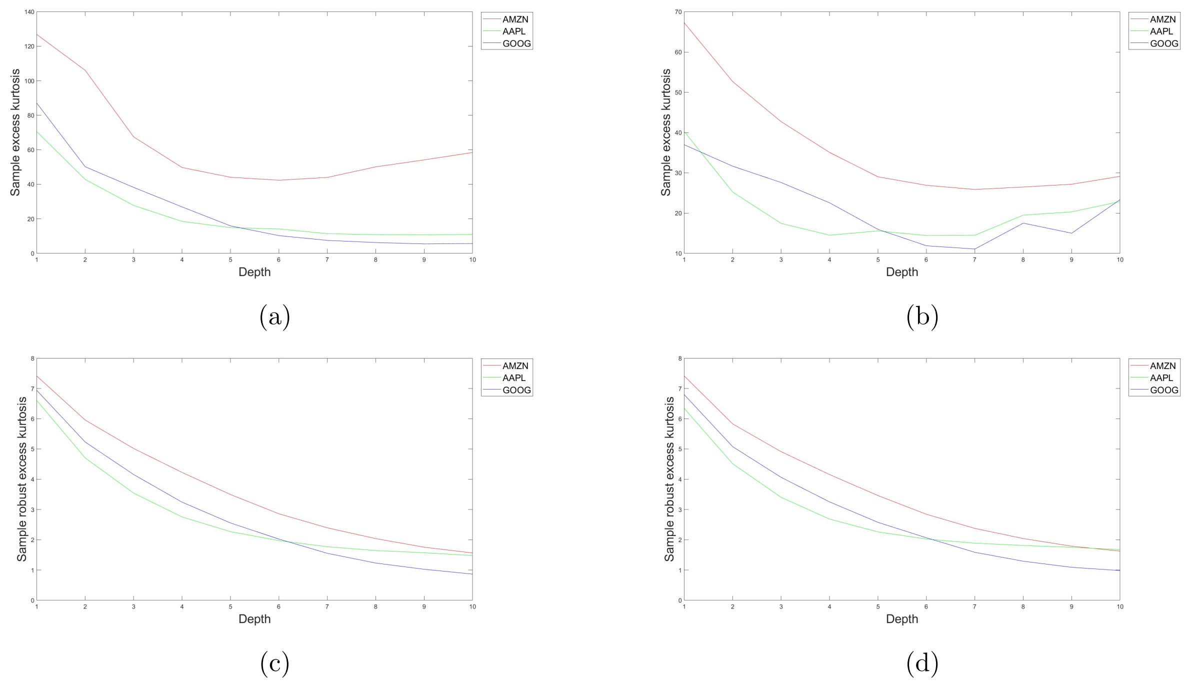

Figure 4: The evolution of excess kurtosis for log-returns of (a) TMOBBAS, (b) GMP and robust excess kurtosis for log-returns of (c) TMOBBAS, (d) GMP over depth (AMZN, AAPL, and GOOG are represented by red, green, and blue line, respectively)

the tail statistics, embodying the principle of "letting the tail speak for itself" ((Embrechts et al., 1997) and (McNeil et al., 2015)).

In the subsequent subsections, we will utilize two methods to show that the distribution of log-returns of TMOBBAS and GMP is heavy-tailed.

4.2 Generalized Pareto Distribution Fit

The initial method we propose involves utilizing the Generalized Pareto Distribution (GPD) to model the tail data of the log-returns. As indicated by (Balkema and De Haan, 1974) and (Pickands III, 1975), a broad category of tail distribution functions can be well approximated by the GPD.

Let $F_{\text{GPD}}(x; \sigma, \xi)$ represent the cumulative distribution function (CDF) of the GPD

$$F_{\text{GPD}}(x; \sigma, \xi) = \begin{cases} 1 - \left(1 + \frac{\xi}{\sigma} x\right)^{-1/\xi} & \text{if } \xi \neq 0 \\ 1 - e^{-x/\sigma} & \text{if } \xi = 0 \end{cases}$$

for $x \in [0, \infty)$ if $\xi \geq 0$ and $x \in [0, -\sigma/\xi]$ if $\xi < 0$. Here, σ is the scale parameter and ξ is the shape parameter. To determine the nature of a distribution's tail, the sign of ξ is crucial. In particular, we have

- If $\xi > 0$, then the distribution has a power-law decay, i.e., heavy-tailed.
- If $\xi = 0$, then the distribution is exponentially decaying.
- If $\xi < 0$, then the distribution has bounded support.

In this study, we consider the top 5% of log-returns data as the tail and employ the GPD to model them. Figure 5 presents a comparison between the empirical CDF of the tail data and the corresponding CDF of the GPD of the TMOBBAS and GMP at all ten depths for AAPL. From Figure 5, it is evident that the overall fit is excellent, allowing us to proceed with this method in our study.

To estimate ξ, a common approach is to utilize maximum likelihood estimation (MLE) ((Davison, 1984), (Smith, 1985), (Smith, 1987), (Hosking and Wallis, 1987), (Grimshaw, 1993), *etc.* among others). By employing the `gpfit()` function in MATLAB, we can calculate the estimated ξ and its 95% confidence interval (CI) for each depth. Figure 6 presents the evolution of the estimated ξ and its corresponding 95% CI across different depths. From Figure 6, we can observe that the estimated ξ are significantly greater than zero, and their corresponding 95% CIs for each depth strictly extend to the right of zero. Thus, we should employ a power-law decay (i.e., heavy-tailed) distribution to fit the entire density of the log-returns of TMOBBAS and GMP.

4.3 The Hill Method

The alternative method we propose is the Hill method. The crucial component in the Hill method is the Hill estimator, introduced by (Hill, 1975). In this method, we will focus on the tail index α, the reciprocal of the shape parameter ξ (i.e., $\alpha = 1/\xi$).

Suppose we have an i.i.d. sample of X with a size of n, $X_1, X_2, \cdots, X_n$, in non-decreasing order, i.e., $X_{(1)} \geq X_{(2)} \geq \cdots \geq X_{(n)}$. The k-th largest value, $X_{(k)}$, is called the k-th order statistic of the sample. The standard form of the Hill estimator is

$$\hat{\alpha}_{k,n}^{(H)} = \left(\frac{1}{k} \sum_{i=1}^{k} \log \frac{X_{(i)}}{X_{(k+1)}} \right)^{-1} = \left[\frac{1}{k} \left(\sum_{i=1}^{k} \log X_{(i)} \right) - \log X_{(k+1)} \right]^{-1}. \tag{6}$$

From Equation (6), we can see that $\hat{\alpha}_{k,n}^{(H)}$ uses only the order statistics up to $k+1$ of the sample to estimate α. Also, from (De Haan and Peng, 1998), we have

$$\hat{\alpha}_{k,n}^{(H)} \xrightarrow{\mathbb{P}} \alpha, \quad \text{if } n \to \infty, k \to \infty, k/n \to 0.$$

This means that the Hill estimator converges in probability to the real tail index when k is chosen appropriately with growing n. From (McNeil et al., 2015), we know that in empirical work, the best choices of k are relatively small–say 10–50 order statistics in a sample of size 1000, i.e., k/n should be about 0.01–0.05.

Besides the Hill estimator itself, we also compute the CI of $\hat{\alpha}_{k,n}^{(H)}$. The $(1-\theta) \times 100\%$ Wald CI (Haeusler and Segers, 2007) can be expressed as

$$I_n^{\text{Wald}}(\theta, k) = \left[\left(1 + \frac{z_{\theta/2}}{\sqrt{k}}\right)^{-1} \hat{\alpha}_{k,n}^{(H)}, \left(1 - \frac{z_{\theta/2}}{\sqrt{k}}\right)^{-1} \hat{\alpha}_{k,n}^{(H)} \right]$$

where z_p means the p-th quantile of the standard Gaussian distribution.

In this study, we let $k/n \approx 0.05$ and $\theta = 0.05$. From Figure 7, we can see that the estimated tail indices are significantly greater than zero and the 95% CIs strictly extend to the right of zero, indicating that the tails are heavy.

5 Dynamics of Log-Returns

In the preceding section, we applied the GPD to characterize the right tails of the logarithmic returns for both TMOBBAS and GMP. Specifically, we identified the top 5% of log-return data as the tail and utilized the GPD to model it. Our analysis included estimating the parameters ξ and the tail

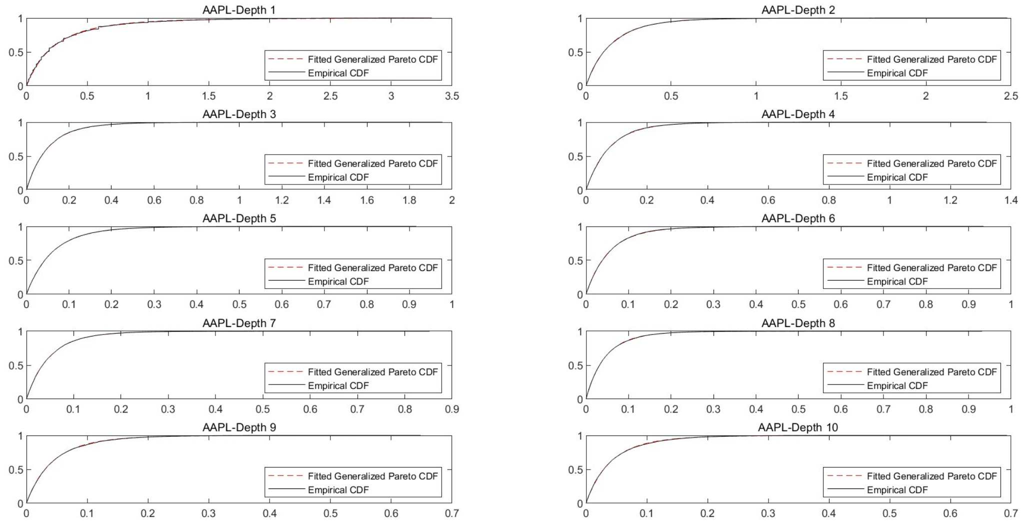

(a)

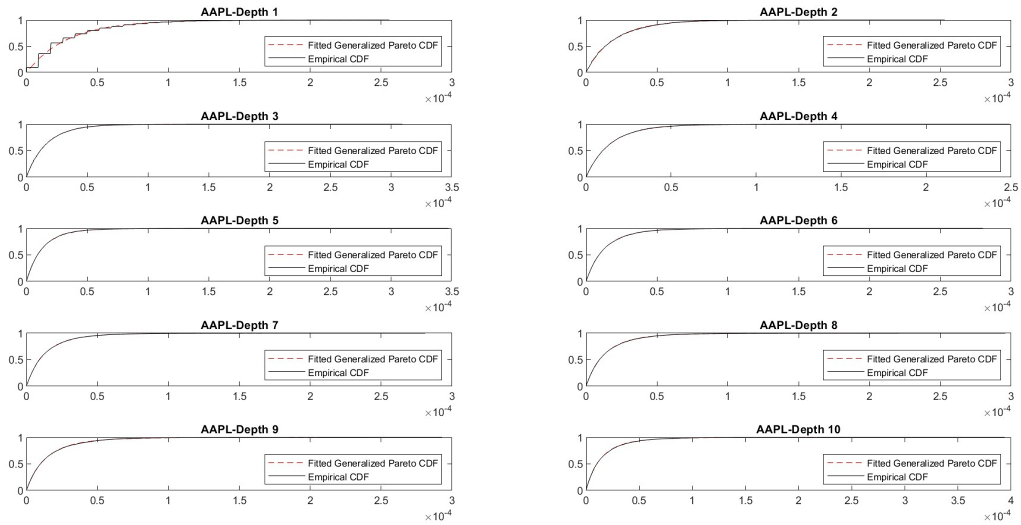

(b)

Figure 5: Comparison between empirical CDF (represented by black solid lines) of tail and its fitted CDF of GPD of (a) TMOBBAS and (b) GMP at all 10 depths for AAPL

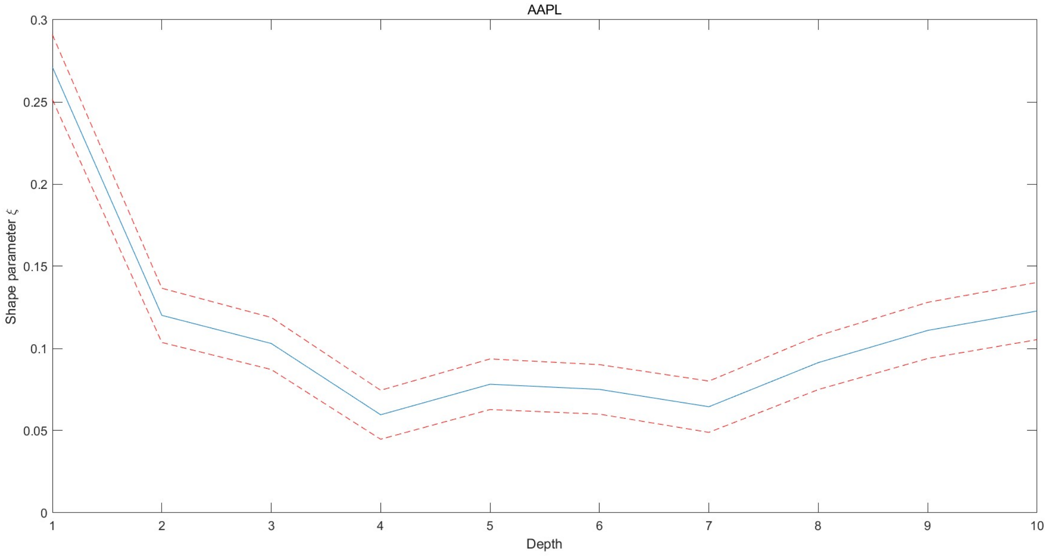

(a)

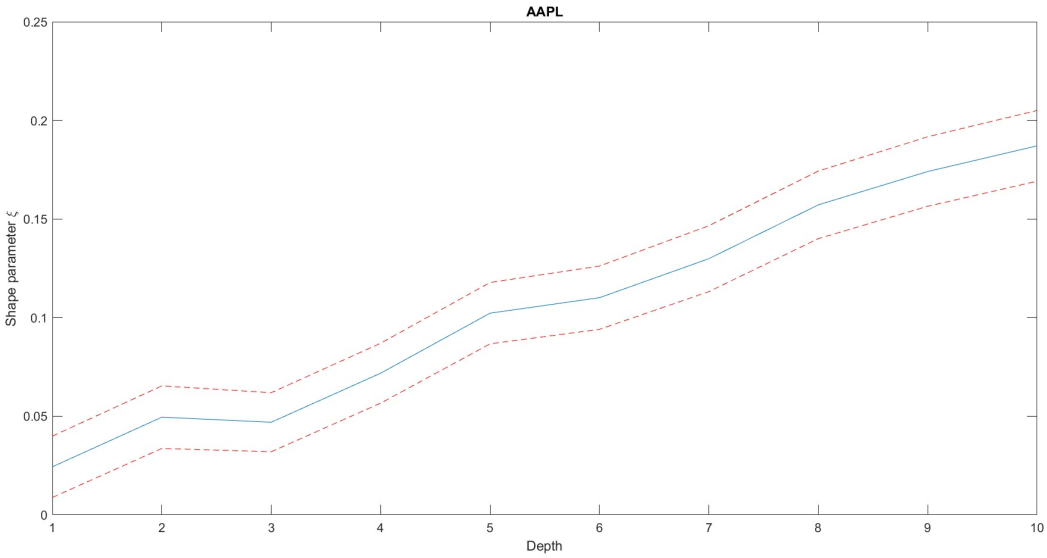

(b)

Figure 6: The evolution of estimated shape parameter ξ (represented by blue solid line) and its corresponding 95% CI (depicted by two red dashed lines) for (a) TMOBBAS and (b) GMP over depth for AAPL

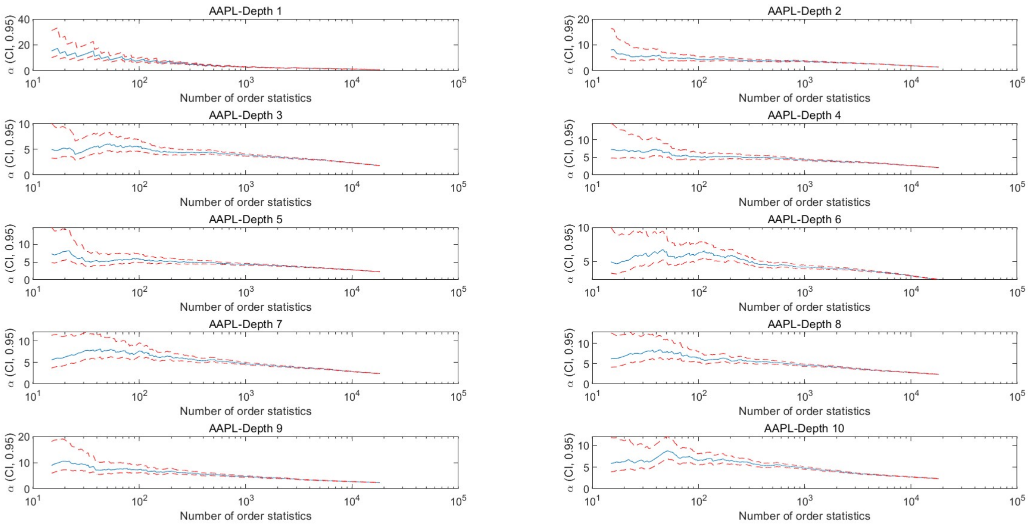

(a)

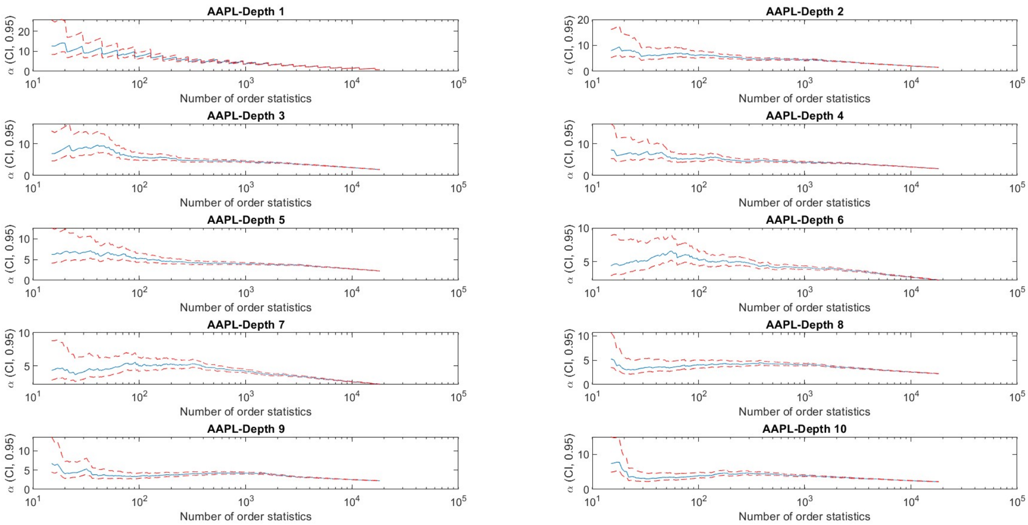

(b)

Figure 7: The dependence of estimated tail index α (represented by blue solid line) and its corresponding 95% CI (depicted by two red dashed lines) for (a) TMOBBAS and (b) GMP on the number of order statistics at all 10 depths for AAPL

index α along with their corresponding 95% confidence intervals for each depth. This revealed that the distributions of the log-returns for both TMOBBAS and GMP exhibit heavy-tailed behavior, indicative of significant deviations from normality.

The methodology employed in the previous sections relied on a historical or static approach, which involved sequentially sampling the returns data from fixed historical periods. This provides a snapshot of market activity and global events within a finite timeframe. Within this framework, we treated the dataset as a series of historical log returns, assuming they were independently and identically distributed. This simplification is widely adopted by practitioners, including traders and portfolio managers, for its simplicity and accessibility. However, it is imperative to acknowledge the common caveat found in fund prospectuses that past performance does not guarantee future returns.

In contrast to the historical approach, dynamic methods investigate more deeply the informational content in the historical data. These methods operate under the assumption that historical returns arise from a dynamic univariate distribution, where characteristics such as dependency may vary over time. Seeking to uncover the nature of this distribution, dynamic methods generate extensive predictive samples of asset returns, with a particular focus on extreme events or tail behavior. The rationale behind using dynamic methods lies in their ability to adapt to changing market conditions and account for evolving risk factors that may not be captured by static models. By continuously updating the model parameters based on new information, dynamic methods offer improved accuracy in predicting future returns and mitigating potential risks. While historical methods remain crucial, especially for modeling new high-frequency spread indices and providing insights into risk management frameworks like Basel I and II, dynamic approaches offer heightened sensitivity to potential significant shifts in market performance. By incorporating the time-varying nature of market dynamics, dynamic methods provide more robust and reliable predictions, making them invaluable tools for investors and risk managers alike.

In this section, we adopt a time-series approach designed to identify the best fitting models for time series data, considering both in-sample and out-of-sample performance. By leveraging Monte Carlo simulations, our goal is to generate a true sample of i.i.d. log-returns for subsequent periods. This methodological shift distinguishes our approach from historical returns, which inherently lack the i.i.d. property.

5.1 ARMA(1,1)–GARCH(1,1) with Normal Inverse Gaussian Distribution

Our dynamic framework incorporates several key components. We utilize a versatile ARMA(1,1)-GARCH(1,1) model to fit the returns data, incorporating a Normal Inverse Gaussian (NIG) distribution to model the innovations within the ARMA-GARCH framework, accommodating heavier tails than a normal distribution. Subsequently, we generate a large sample of asset innovation values from the NIG distribution. By applying inverse ARMA-GARCH to this sample set, we derive a comprehensive set of values of the returns. These values are then incorporated into our analysis to model spread indices across various depths of the order book, providing deeper insights into market dynamics and risk management strategies. Additionally, we aim to employ the same dynamic framework for analyzing the GMP data alongside TMOBBAS to enhance the comprehensiveness of our analysis.

If a time-series of returns, r_t, is stationary, a useful general model for describing it is the synthesis of the autoregressive moving-average (ARMA) model and the generalized autoregressive conditional heteroscedasticity (GARCH) model. The ARMA (Eagle, 1982) component explicitly models the behavior of the returns, whereas the GARCH (Bollerslev, 1986) component explicitly models its variance. Both models contain theoretically infinite parameters; the variations in the models are denoted by the finite number of parameters employed. The ARMA(p, q) model (Tsay, 2005) is

$$r_t = \phi_0 + \sum_{i=1}^{p} \phi_i r_{t-i} + a_t + \sum_{j=1}^{q} \theta_j a_{t-j},$$

where each shock, a_t, is a zero-mean random variable. The first two terms in Equation (7) describe the autoregressive dependence of r_t on previous returns; the second two terms add the influence of a weighted (moving) average of shocks, a_t. The GARCH(m, s) model relates a_t to, and provides a model for, the variance σ_t^2 of the series:

$$a_t = \sigma_t \epsilon_t, \quad \sigma_t^2 = \alpha_0 + \sum_{i=1}^{m} \alpha_i a_{t-i}^2 + \sum_{j=1}^{s} \beta_j \sigma_{t-j}^2. \tag{7}$$

Here, the so-called innovations, ϵ_t, are zero-mean, unit-variance, independent, identically distributed random variables. The GARCH model is clearly autoregressive in both σ_t^2 and a_t^2.

Identifying the daily variance as the volatility of the time series, Equation (7) captures the property of conditional heteroscedasticity, that is, the property that the volatility is not constant relative to that of prior days. With six parameters, the ARMA(1,1)–GARCH(1,1) model

$$\begin{aligned}
r_t &= \phi_0 + \phi_1 r_{t-1} + a_t + \theta_1 a_{t-1}, \\
a_t &= \sigma_t \epsilon_t, \\
\sigma_t^2 &= \alpha_0 + \alpha_1 a_{t-1}^2 + \beta_1 \sigma_{t-1}^2,
\end{aligned}$$

provides enough generality to model many time series of returns. However, providing a fit to a particular time series requires the specification of the distribution governing the random variables of the innovations. In the dynamic optimization method, we assume that the innovations, ϵ_t, are governed by the NIG distribution given by

$$f(x|\alpha, \beta, \mu, \delta) = \frac{\delta}{2\alpha K_1(\delta)} \exp\left(-\frac{\delta}{\alpha}\left(\sqrt{\beta^2 + (x-\mu)^2} - \sqrt{\beta^2 + \mu^2}\right)\right),$$

where $K_1(\cdot)$ is the modified Bessel function of the second kind, and α, β, μ, and δ are shape and scale parameters.

5.2 The TMOBBAS Hill Index Estimations

The dynamic module seeks to provide a statistically accurate larger sampling of returns for computing the tail index. This is achieved by fitting an ARMA(1,1)–GARCH(1,1) with an NIG-distribution model to the time series of the TMOBBAS index of depths $s = 1, 2, ..., 10$, generating the model parameters, computing the shock series a_t and the variances σ_t^2 predicted from the fitted GARCH(1,1) model, generating $10,000$ of the innovation series ϵ_t, and performing the inverse transformations ϵ_t in the ARMA(1,1)–GARCH(1,1) model to generate a dynamic ensemble of predicted returns for the TMOBBAS index for each depth. The ensemble of returns $\{r_t^{(s)}\}_{s=1}^{10}$ represents the output from the dynamic module, which is then incorporated into our analysis to model spread indices across various depths of the order book, providing deeper insights into market dynamics and risk management strategies.

Figure 8 illustrates the evolution of the estimated ξ and its corresponding 95% CI across different depths. From Figure 8, we observe that the estimated values of ξ are significantly greater than zero, and their corresponding 95% CIs for each depth strictly extend to the right of zero. Thus, we should consider a power-law decay (i.e., heavy-tailed) distribution to fit the entire density of the log-returns of the TMOBBAS and confirm our findings with the historical methodology.

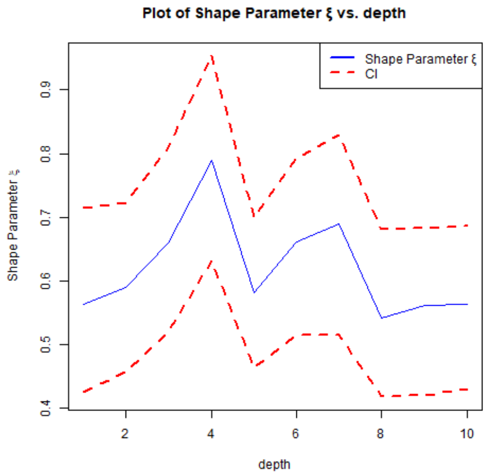

Figure 8: The evolution of estimated shape parameter ξ (represented by blue solid line) and its corresponding 95% CI (depicted by two red dashed lines) over depth for AAPL

For estimating the Hill index for each depth, consistent with our historical methodology, we set $k/n \approx 0.05$ and $\theta = 0.05$. From Figure 9, it is evident that the estimated tail indices are significantly greater than zero, with the 95% confidence intervals extending strictly to the right of zero. This observation indicates that the tails of the distribution should be characterized as heavy-tailed, corroborating our findings from the historical methodology.

Furthermore, in Figure 9, we observe a decreasing trend in the evolution of the estimated tail index α and its associated confidence intervals as a function of the number of order statistics. As we include more extreme values (higher order statistics), the variability in the estimates of the tail index decreases, leading to a more conservative estimate. In other words, a larger number of order statistics results in a more robust estimation, yielding a stable and lower estimate of the tail index.

Furthermore, we examined the tail behavior of an Equally Weighted Portfolio (EWP) comprising returns from all ten depths. Adopting an EWP approach facilitated the aggregation of returns across multiple depths, offering a holistic view of market behavior while minimizing the influence of individual depth-specific factors. As illustrated in Figure 10, our analysis reaffirms the heavy-tailed nature of the distribution, indicating significant deviations from normality. This observation underscores the robustness of our methodology in capturing heavy-tailed behavior across the TMOBBAS index, further enhancing our understanding of tail risk dynamics within the market.

These findings from our analysis provide valuable insights into the tail behavior of the log-returns for the TMOBBAS index, particularly when comparing results obtained from historical methodologies with dynamic approaches. Our examination of the Hill index for each depth, consistent with our historical methodology, reaffirms the heavy-tailed nature of the distribution.

5.3 The GMP Hill Index Estimations

In this subsection, we extend our analysis to the GMP, applying the same methodology previously employed for the analysis of the TMOBBAS. By leveraging the dynamic framework described earlier, we aim to provide insights into the tail behavior and dynamics of GMP returns across various depths of the order book.

The dynamic module utilized an ARMA(1,1)–GARCH(1,1) model a NIG distribution to fit the time series of the GMP index for depths $s = 1, 2, ..., 10$. This generated a statistically accurate ensemble of predicted returns for GMP at each depth, facilitating the modeling of spread indices and offering deeper insights into market dynamics and risk management strategies.

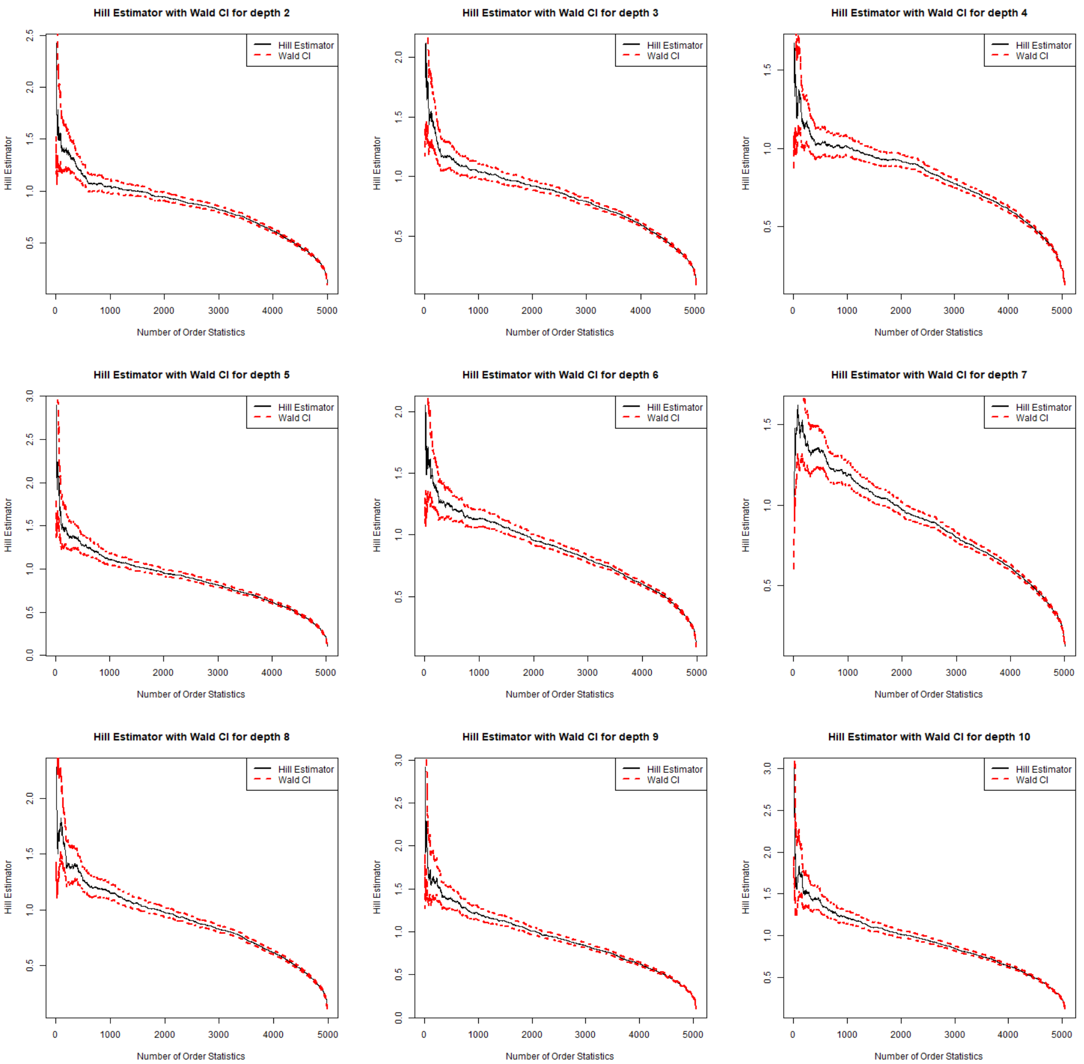

Figure 9: The dependence of estimated tail index α (represented by black solid lines) and its corresponding 95% CI (depicted by two red dashed lines) on the number of order statistics at depths 2, 3, $\cdots$ 10 for AAPL

We estimated the Hill index for each depth of the GMP, consistent with our methodology applied to TMOBBAS. Figure 11 demonstrates the evolution of the estimated tail index α and its corresponding 95% confidence intervals on the number of order statistics at each depth for GMP.

Additionally, we examined the tail behavior of an EWP comprising returns from all ten depths of the GMP. This approach allowed us to gain a comprehensive understanding of market behavior while mitigating the influence of individual depth-specific factors. Figure 12 presents the evolution of the estimated tail index α and its corresponding 95% confidence intervals on the number of order statistics for the EWP of GMP.

By conducting a thorough analysis of the GMP using the established methodology, we aim to enhance our understanding of market dynamics and tail risk within the context of the order book. This analysis complements our investigation of TMOBBAS and GMP, providing valuable insights into the behavior of both indices and informing effective risk management strategies in financial markets.

Furthermore, by comparing the analyses of the tail behavior of GMP and TMOBBAS, we observe

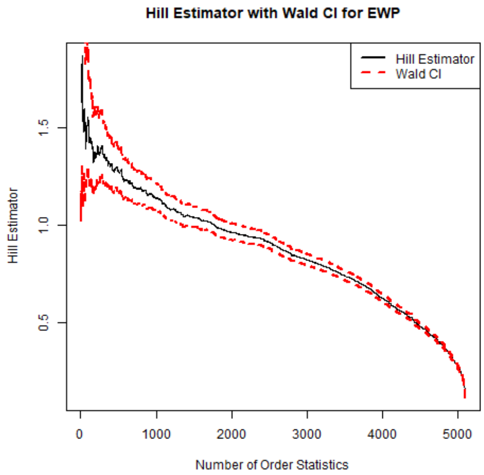

Figure 10: The dependence of estimated tail index α (represented by black solid line) and its corresponding 95% CI (depicted by two red dashed lines) on the number of order statistics for EWP for AAPL

that while there are similar trends in the shape of their tail indices, there are also notable differences, suggesting distinct risk profiles for each index. It is worth noting that the Hill index estimated for all depths of GMP shows very similar values, with minimal variation. This observation contrasts with the behavior observed for TMOBBAS, where the Hill index varies significantly between depths, ranging from 0 to 3. The consistent behavior of the Hill index as a function of depth for GMP suggests a more stable tail behavior compared to TMOBBAS.

This phenomenon may be due to the nature of the market and the characteristics of the order book. The GMP may exhibit a more uniform distribution of returns across depths, leading to consistent tail behavior. On the other hand, the TMOBBAS may experience more variability in trading activity and liquidity across depths, resulting in fluctuating tail behavior.

This analysis complements our investigation of TMOBBAS and GMP, providing valuable insights into the behavior of both indices and informing effective risk management strategies in financial markets.

6 Option Pricing and Implied Volatility

The primary objective of our paper is to introduce and analyze the new high-frequency spread indices, TMOBBAS and GMP, which capture the dynamics of variations in the spread across different depths of the order book. Our findings from previous sections show that the log-returns and spreads at different depths exhibit heavy-tailed characteristics, highlighting the potential challenges faced by market participants, particularly high-frequency traders, who are sensitive to fluctuations in liquidity.

As we investigated the analysis of both TMOBBAS and GMP, it became evident that global spreads and mid-prices at various depths can significantly vary, thereby impacting liquidity. This observation underscores the potential challenges faced by market participants, particularly high-frequency traders, who are sensitive to fluctuations in liquidity. In response to this concern, there arises an opportunity to explore innovative risk management strategies. One such approach involves the adoption of insurance instruments akin to portfolio insurance, aimed at hedging against the risk of low liquidity.

Thus, there is a compelling rationale for the development of an option pricing model tailored specifically for spreads at different levels. By constructing an equally weighted index comprising

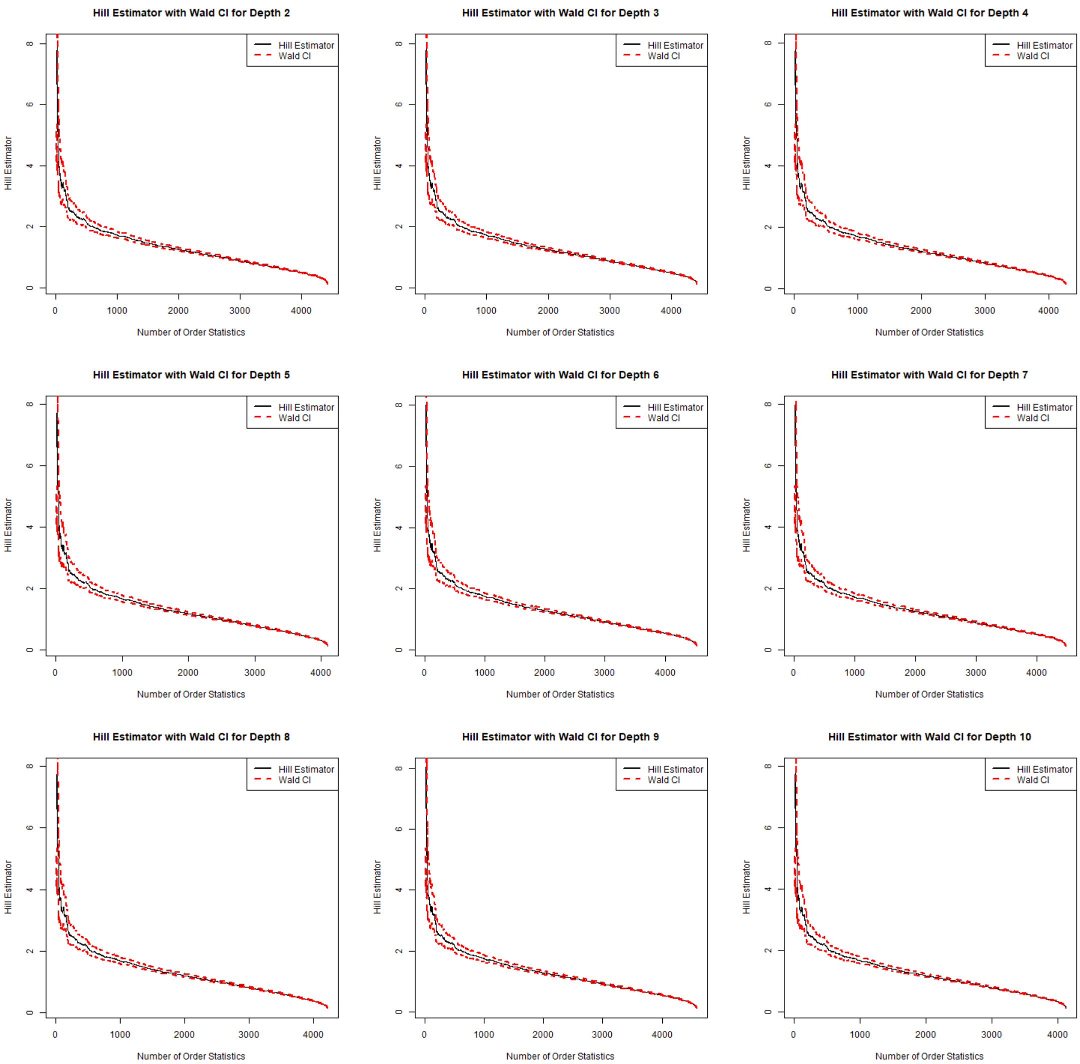

Figure 11: The dependence of estimated tail index α (represented by black solid lines) for GMP and its corresponding 95% CI (depicted by two red dashed lines) on the number of order statistics at depth $2,3,\cdots$ 10 for AAPL

these spreads and offering derivative pricing on this index, we can furnish market participants with a robust mechanism for hedging against the adverse effects of low liquidity. This initiative not only addresses the practical needs of traders but also contributes to the ongoing discourse on risk management in financial markets.

This section focuses on pricing options on both the TMOBBAS and GMP indices and deriving their implied volatilities. Measures of implied volatility play a crucial role in this context by encapsulating the current perspective of the market on the future risk, as implied by the observed transaction prices of option contracts. Given the dynamic nature of the high-frequency market and the presence of temporal dependence, as manifested in volatility clustering, traditional measures of historical volatility may be inadequate for capturing the prevailing risk environment. Implied volatility offers a forward-looking outlook, integrating market expectations and sentiments, thereby furnishing valuable insights for traders and investors.

Our approach involves employing a double-subordinated process to model both the TMOBBAS and GMP indices. This method is chosen to enhance the accuracy and reliability of the pricing,

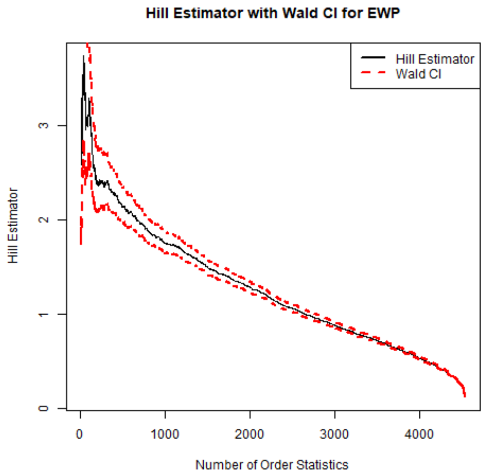

Figure 12: The dependence of estimated tail index α (represented by black solid line) of GMP and its corresponding 95% CI (depicted by two red dashed lines) on the number of order statistics for EWP for AAPL

particularly in capturing the dynamic nature of the high-frequency market and addressing the challenges associated with the heavy-tailed distributions of asset returns. This choice is informed by empirical evidence suggesting that the returns of speculative assets, such as the TMOBBAS and GMP indices, are heavy-tailed distributions and asymmetric, challenging the assumption of normality underlying traditional option pricing models like the Black–Scholes–Merton (BSM) formula. A double-subordinated process enables the variance of the normal distribution to vary over time, thereby effectively capturing heavy-tailed phenomena. Specifically, one of the subordinated processes models intrinsic time, enhancing our ability to capture the intricate dynamics of both the TMOBBAS and GMP indices and provide more accurate pricing for options based on them.[3]

6.1 Double Subordination Model for TMOBBAS and GMP

In this subsection, we define the double-subordinated process for modeling both the TMOBBAS and GMP indices and pricing options based on their dynamics. By outlining the model parameters and processes, we lay the groundwork for our analysis, aiming to capture the nuanced behavior of these indices and provide accurate pricing for options, contributing to risk management and investment strategies in the high-frequency trading domain. Through this exploration, we aim to uncover valuable insights into the dynamics of both the TMOBBAS and GMP indices and their implications for market participants.[4]

The double-subordination framework involves a Lévy subordinator process, denoted by $\mathbb{X} = (X(t), t \geq 0)$, defined on a stochastic basis $(\Omega, \mathcal{F}, \mathbb{F}, \mathbb{P})$. A process $\mathbb{X}$ is considered a Lévy process if $X(0) = 0$ almost surely under $\mathbb{P}$, it has independent increments, has stationary increments, and is continuous in probability. [5] A Lévy process $\mathbb{T} = (T(t),\ t \geq 0,\ T(0) = 0)$ with non-decreasing trajectories (i.e., non-decreasing sample paths) is called a *Lévy subordinator*. Since $T(0) = 0$, the trajectories of $\mathbb{T}$ take only non-negative values. In the BSM option pricing model, the price dynamics

[3]For a further discussion of the use of subordinators in financial modeling, see (Sato, 1999), (Schoutens, 2003), and (Shirvani et al., 2021a).

[4]For more details on Lévy subordinator processes, refer to (Duffie, 2010).

[5]For more details on Lévy subordinator processes, refer to (Sato, 1999) and (Schoutens, 2003).

of the underlying asset are given by

$$S_t^{(\mathrm{BSM})} = e^{X_t^{(\mathrm{BSM})}}, \quad t \in [0, \tau],$$

where the log-process is

$$X_t^{(\mathrm{BSM})} = X_0 + \mu_1 t + \sigma_1 B_t, \quad \mu_1 \in \mathbb{R},\ \sigma_1 > 0,\ X_0 = \ln(S_0),\ S_0 > 0,$$

and $\mathbb{B} = (B_t,\ t \geq 0)$ is a standard Brownian motion. To accommodate the non-normality of asset returns, (Mandelbrot and Taylor, 1967) and (Clark, 1973) proposed the use of a subordinated Brownian motion, where the price process $S_t^{(\mathrm{ss})}$ and the log-price process are defined by

$$S_t^{(\mathrm{ss})} = e^{X_t^{(\mathrm{ss})}}, \quad t \in [0, \tau],$$
$$X_t^{(\mathrm{ss})} = X_0 + \mu_2 t + \sigma_2 B_{T(t)}, \quad \mu_2 \in \mathbb{R},\ \sigma_2 > 0, \tag{8}$$

where $\mathbb{T} = (T(t),\ t \geq 0,\ T(0) = 0)$ is a Lévy subordinator.

Various studies have demonstrated that single-subordinated log-price models commonly fail to capture the heavy-tailedness observed in financial returns.[6] (Shirvani et al., 2021a) defined and investigated the properties of various multiple-subordinated log-return processes designed to model leptokurtic asset returns. They showed that multiple-subordinated log-return processes can have heavier tails than single-subordinated models and that they are capable of capturing skewness and kurtosis. Therefore, a double subordination framework may be a more appropriate candidate for modeling the rather extreme behavior of both the TMOBBAS and GMP indices.

To apply double subordination to modeling the TMOBBAS and GMP index price processes, let S_t denote the price process with the dynamics

$$\begin{gathered} S_t = e^{X_t}, \quad t \in [0, \tau], \\ X_t = X_0 + \mu_3 t + \gamma U(t) + \rho T(U(t)) + \sigma_3 B_{T(U(t))}, \quad t \geq 0, \\ \mu_3 \in \mathbb{R},\ \sigma_3 > 0,\ X_0 = \ln(S_0),\ S_0 > 0. \end{gathered} \tag{9}$$

where the components of the triple $B_s, T(s), U(s), s \geq 0$ are independent processes generating the stochastic basis $(\Omega, \mathcal{F},\ \mathbb{F} = (\mathcal{F}_t, t \geq 0), \mathbb{P})$, which represents the real world.

Consider the case where the subordinators $T(t)$ and $U(t)$ are inverse Gaussian (IG) Lévy processes; In this case, (Shirvani et al., 2021a) referred to $T(U(t))$ as the *double inverse Gaussian subordinator* and to X_t as a *normal double inverse Gaussian (NDIG) log-price process*, with the characteristic function (CF) of X_1 given by

$$\varphi_{X_1}(v) = \exp\left\{ iv\mu_3 + \frac{\lambda_U}{\mu_U}\left[1 - \sqrt{1 - \frac{2\mu_U^2}{\lambda_U}\left(\frac{\lambda_T}{\mu_T}\left(1 - \sqrt{1 - \frac{\mu_T^2}{\lambda_T}(2iv\rho - \sigma_3^2 v^2)}\right) + iv\lambda\right)}\right]\right\}, \tag{10}$$

with $v \in \mathbb{R}$.

To price European contingent claims of both TMOBBAS and GMP indices, we follow (Shirvani et al., 2023) and assume that the log-price process X_t follows a NDIG model. An equivalent martingale measure $\mathbb{Q}$ is derived from the risk-neutral measure $\mathbb{P}$, ensuring that the discounted price process $e^{-rt}S_t$ is a martingale (Duffie, 2010, Chapter 6). Using the martingale-corrected moment matching

[6] For example, see (Lundtofte and Wilhelmsson, 2013) and (Shirvani et al., 2021b).

(MCMM) approach, the parameters of the process are estimated, and an appropriate drift term is added to ensure the martingale property.[7]

The price of a European call option $\mathcal{C}$ with an underlying asset $\mathcal{S}$ is given by

$$C(S_0, r, K, \tau) = e^{-r\tau}\ \mathbb{E}_{\mathbb{Q}}\left[\max(S_\tau^{(\mathbb{Q})} - K, 0)\right],$$

where τ denotes the maturity, K is the strike price, and $S_t^{(\mathbb{Q})}$ is the price dynamics of $\mathcal{S}$ under $\mathbb{Q}$. (Shirvani et al., 2023) dervied the price dynamics of $\mathcal{S}$ under $\mathbb{Q}$ and the CF of the log-price $\ln S_t^{(\mathbb{Q})}$, respectively, given by

$$S_t^{(\mathbb{Q})} = \frac{b_t S_t}{M_{X_t}(1)} = S_0 e^{\left(r - K_{X_1}(1)\right)t + X_t}, \quad t \in [0, \tau], \tag{11}$$

$$\varphi_{\ln S_t^{(\mathbb{Q})}}(v) = S_0^{iv} \exp\left\{\left[iv(r - K_{X_1}(1)) + \psi_{X_1}(v)\right] t\right\}, \quad t \in [0, \tau]. \tag{12}$$

The efficient computation of option prices relies on (Carr and Madan, 1998)'s option pricing formula, utilizing the fast Fourier transform (FFT) and necessitating access to the CF of the log-price, represented by

$$C(S_0, r, k, \tau) = \frac{e^{-r\tau - ak}}{\pi} \int_0^\infty e^{-ivk} \frac{\varphi_{\ln S_\tau^{(\mathbb{Q})}}(v - i(a+1))}{a^2 + a - v^2 + i(2a+2)v} dv, \tag{13}$$

where $a > 0$ and $E(S_t^{(\mathbb{Q})})^a < \infty$. [8]

For pricing options on both the TMOBBAS and GMP indices and deriving their implied volatility, we employ a double-subordinated process to model these indices. The method of moments and the empirical CF are utilized to estimate the parameters of the model, following (Paulson et al., 1975) and (Yu, 2003).[9]

6.2 Option Pricing and Implied Volatility of TMOBBAS

To explore the realm of option pricing and implied volatility for the TMOBBAS index, we employ the NDIG Lévy model. This model facilitates the pricing of plain vanilla European options on the TMOBBAS index, providing valuable insights into market dynamics and risk management strategies. Let's explore the details.

We apply the NDIG Lévy model to the pricing of plain vanilla European options on the TMOBBAS index. Let $\mathcal{C}$ be a European call option, where the underlying risky asset $\mathcal{S}$ follows the log-price process given in Equation (9). The dynamics of $\mathcal{S}$ on $\mathbb{Q}$ are given by Equation (11), and the CF of the log-price is given by Equation (12). We evaluate the integral Equation (13) using the FFT for a range of strike levels and maturity horizons.

Figure 13 depicts the resulting prices for call and put options plotted against the time to maturity τ and the strike price K for depths 5 and 10. Since the call and put surfaces for different depths of the TMOBBAS index are similar, we only plot the TMOBBAS index with depths 5 and 10.

[7](Yao et al., 2011) constructed a martingale measure using the MCMM approach for the geometric Lévy process model and showed that this measure is an equivalent martingale measure if there is a continuous Gaussian part in the Lévy process. If X_t is a pure-jump Lévy process, they pointed out that this measure cannot be equivalent to a physical probability. However, pricing European options under this measure is still arbitrage-free.

[8]Limits for a ensuring stable option prices are determined through numerical experiments, see (Shirvani et al., 2023).

[9]Exploiting the fact that the probability density function (PDF) is the Fourier transform of the CF, the objective is to minimize the squared differences of the first four moments and the empirical and theoretical CFs. This involves estimating model parameters through optimization subject to constraints based on the statistical properties of the data. See (Shirvani et al., 2023).

It's worth noting that for close-to-the-money values ($K \approx S$), where the strike price is close to the current asset price, the call and put option prices increase with τ, reflecting increased future uncertainty. This behavior is consistent with market expectations, as higher uncertainty about the future value of the underlying asset leads to higher option prices. This phenomenon is often observed in financial markets, where options with longer maturities tend to command higher premiums due to the additional time value and increased uncertainty associated with longer time horizons.

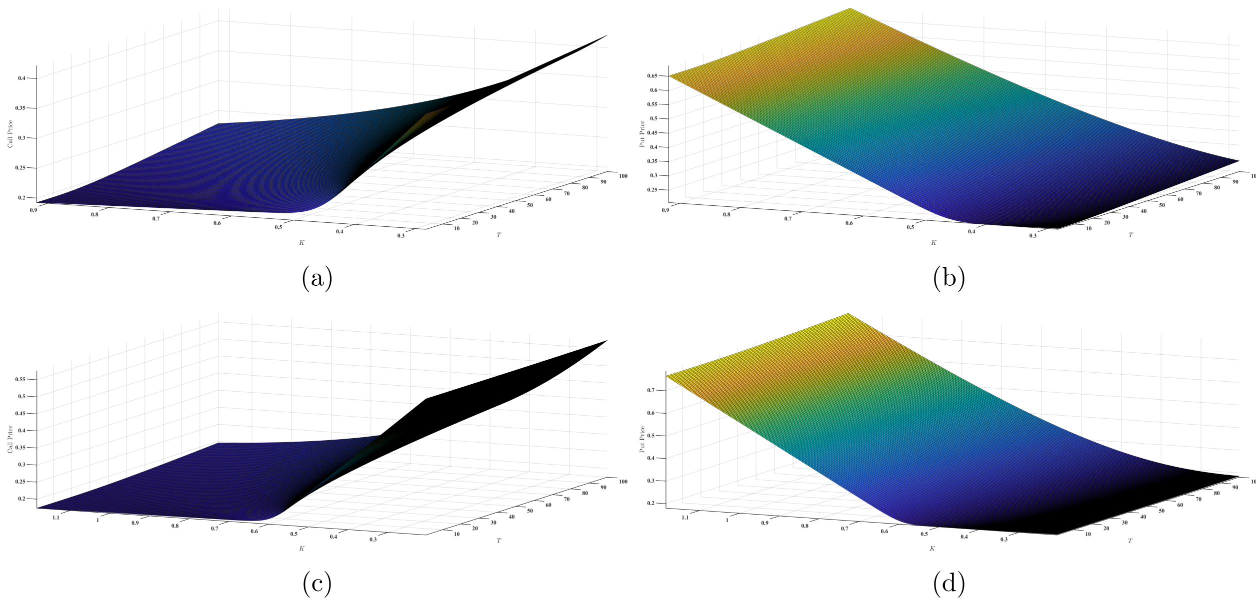

Figure 13: NDIG-based call price surfaces for TMOBBAS index of AAPL (a) for depth 5, (b) for depth 5, (c) for depth 10, and (d) for depth 10 as functions of the time to maturity and strike price.

Figures 14 and 15 also plot the implied volatility surface computed from call price options for the TMOBBAS index for depths 1 to 10 and EWP as a function of T and moneyness, K/S_0. As is typically observed, at constant values of T the implied volatility (future uncertainty) increases as strike prices move away from the value K/S_0 (the volatility "smile"). At constant values of K/S_0, the implied volatility decreases as time to maturity increases.

We also observe a decrease in implied volatility as depth increases, as illustrated in Figure 14, which presents an intriguing trend in the context of option pricing dynamics for the TMOBBAS index. Market depth, representing the level of liquidity and trading activity, plays a crucial role in determining option prices and their associated implied volatilities.

The decrease in implied volatility with increasing depth suggests a relationship between market depth and option pricing stability. Deeper markets typically exhibit higher liquidity, characterized by a larger volume of buy and sell orders across various price levels. This increased liquidity contributes to a more stable and efficient pricing environment, reducing the uncertainty surrounding future price movements. As a result, options priced in deeper markets tend to reflect lower implied volatility levels, as market participants perceive less risk and uncertainty in price fluctuations.

Moreover, deeper markets often feature narrower bid–ask spreads, indicating tighter pricing and improved market efficiency. The reduced spread suggests that buyers and sellers are more closely aligned in their pricing expectations, further contributing to the lower implied volatility observed in options priced based on the TMOBBAS index.

Additionally, our analysis reveals a striking similarity between the implied volatility surface of the EWP encompassing all depths of the TMOBBAS index and the implied volatility of the TMOBBAS index with depth 10. This observation suggests that the implied volatility of the EWP, which

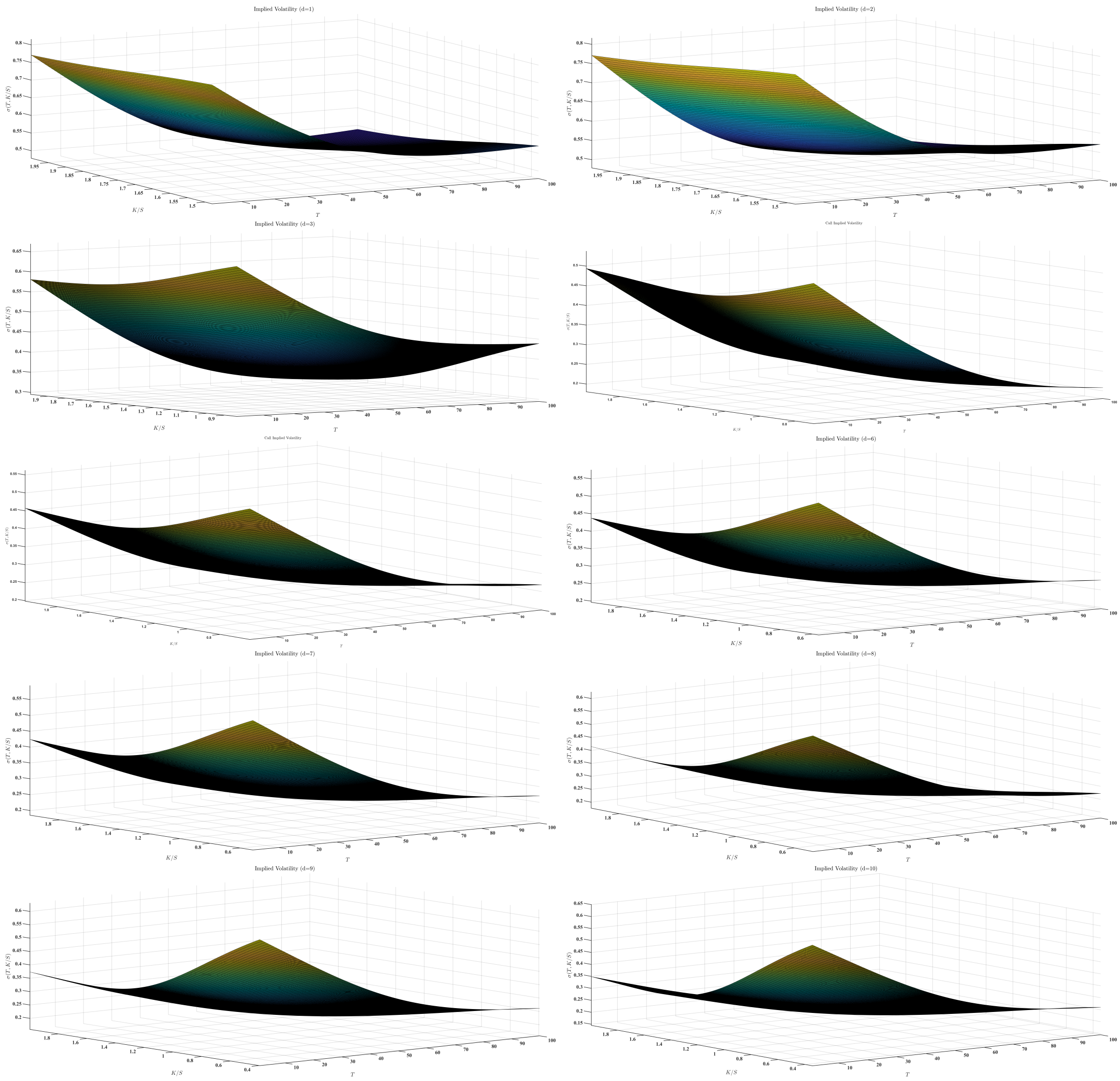

Figure 14: Implied volatility surface for depths $1, 2, ..., 10$ for AAPL

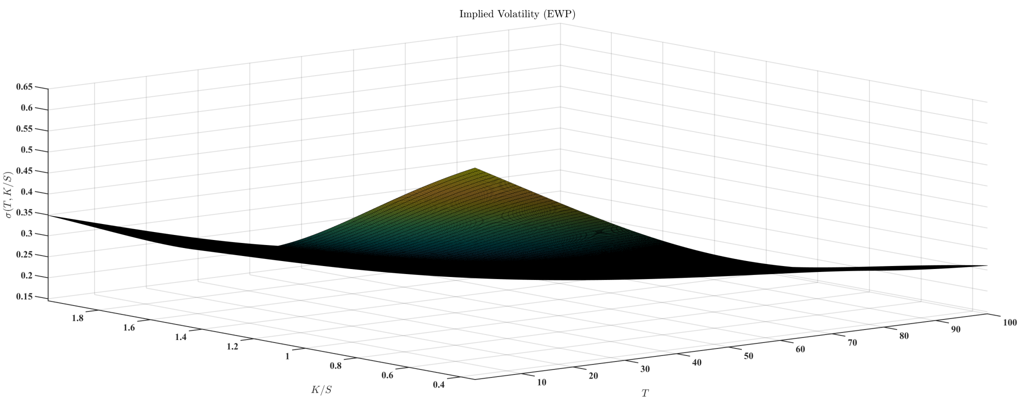

Figure 15: Implied volatility surface for EWP

aggregates returns from all depths, closely mirrors the implied volatility behavior of the TMOBBAS index with the greatest market depth. Essentially, the EWP serves as a holistic representation of market sentiment and volatility by amalgamating information from diverse depths of the TMOBBAS index. Consequently, the implied volatility surface of the EWP offers a comprehensive perspective on market volatility, integrating insights from various depths.

Moreover, the notable resemblance between the implied volatility of the EWP and the TMOBBAS index with depth 10 indicates the predominant influence of deeper market levels on overall market volatility. This underscores the critical role of deep liquidity levels in shaping market sentiment and option pricing dynamics. The convergence of implied volatility behavior between the EWP and the TMOBBAS index with the greatest depth underscores the importance of considering depth-specific factors in understanding and predicting market volatility.

To summarize, the inverse relationship between implied volatility and market depth underscores the importance of liquidity and stability in option pricing. The decreasing trend in implied volatility with increasing depth highlights the role of deeper markets in providing a more stable and predictable pricing environment for options, benefiting both investors and market participants alike. Furthermore, the remarkable resemblance between the implied volatility of the EWP encompassing all depths of the TMOBBAS index and the TMOBBAS index with depth 10 suggests that deeper market levels have a dominant influence on overall market volatility, emphasizing the significance of high levels of liquidity in shaping market sentiment and option pricing dynamics.

6.3 Option Pricing and Implied Volatility of GMP

In this subsection, we present the results of analyzing option pricing and implied volatility for the GMP index, leveraging the NDIG Lévy model. Our objective is to gain insights into the pricing dynamics of plain vanilla European options on the GMP index and assess implied volatility trends.

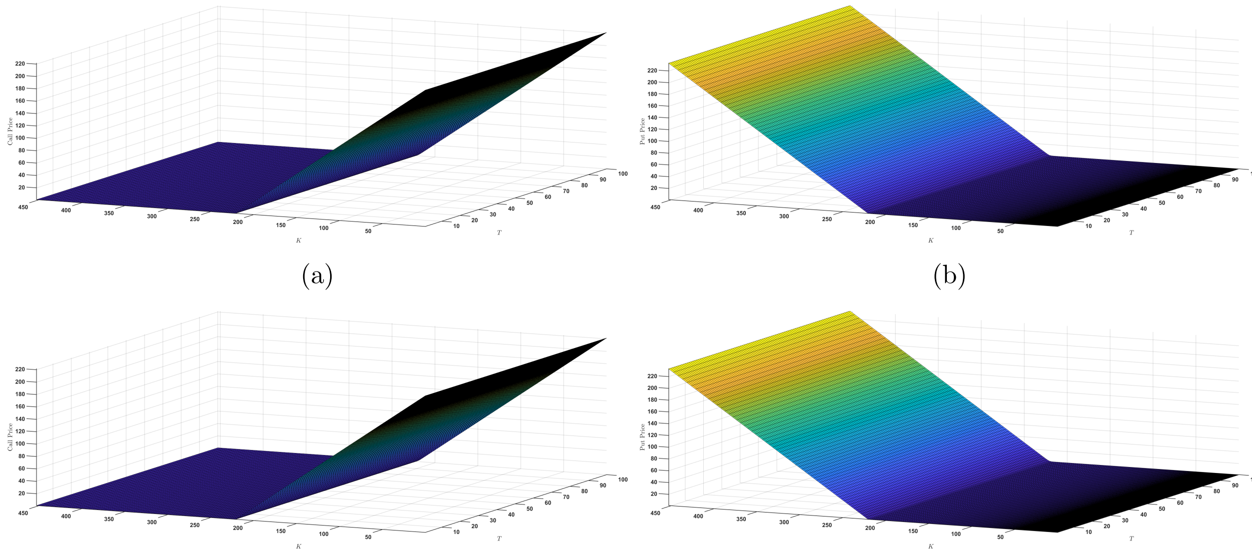

(a) (b)

(c) (d)

Figure 16: NDIG-based call price surfaces for TMOBBAS index of AAPL (a) for depth 5, (b) for depth 5, (c) for depth 10, and (d) for depth 10 as functions of the time to maturity and strike price.

Figure 16 showcases the pricing surfaces for call and put options plotted against the time to maturity τ and the strike price K, focusing on depths 5 and 10 of the GMP index. Notably, these surfaces offer valuable insights into the option pricing behavior specific to the GMP index.

Observing the patterns in the pricing surfaces reveals intriguing dynamics. Particularly, for near-the-money options ($K \approx S$), where the strike price closely aligns with the current asset price, both call and put option prices demonstrate an increasing trend with τ. This trend reflects the market's anticipation of heightened future uncertainty, leading to elevated option premiums for longer-maturity contracts. Such observations align with established market phenomena, where longer-maturity options command higher premiums due to increased time value and augmented uncertainty associated with extended time horizons.

Figures 17 and 18 depict the implied volatility surface computed from call price options for the GMP index across depths 1 to 10 and EWP as a function of T and moneyness, K/S_0. Notably, the implied volatility exhibits a distinct "smile" pattern, characterized by a sharp increase in volatility as the moneyness approaches zero.

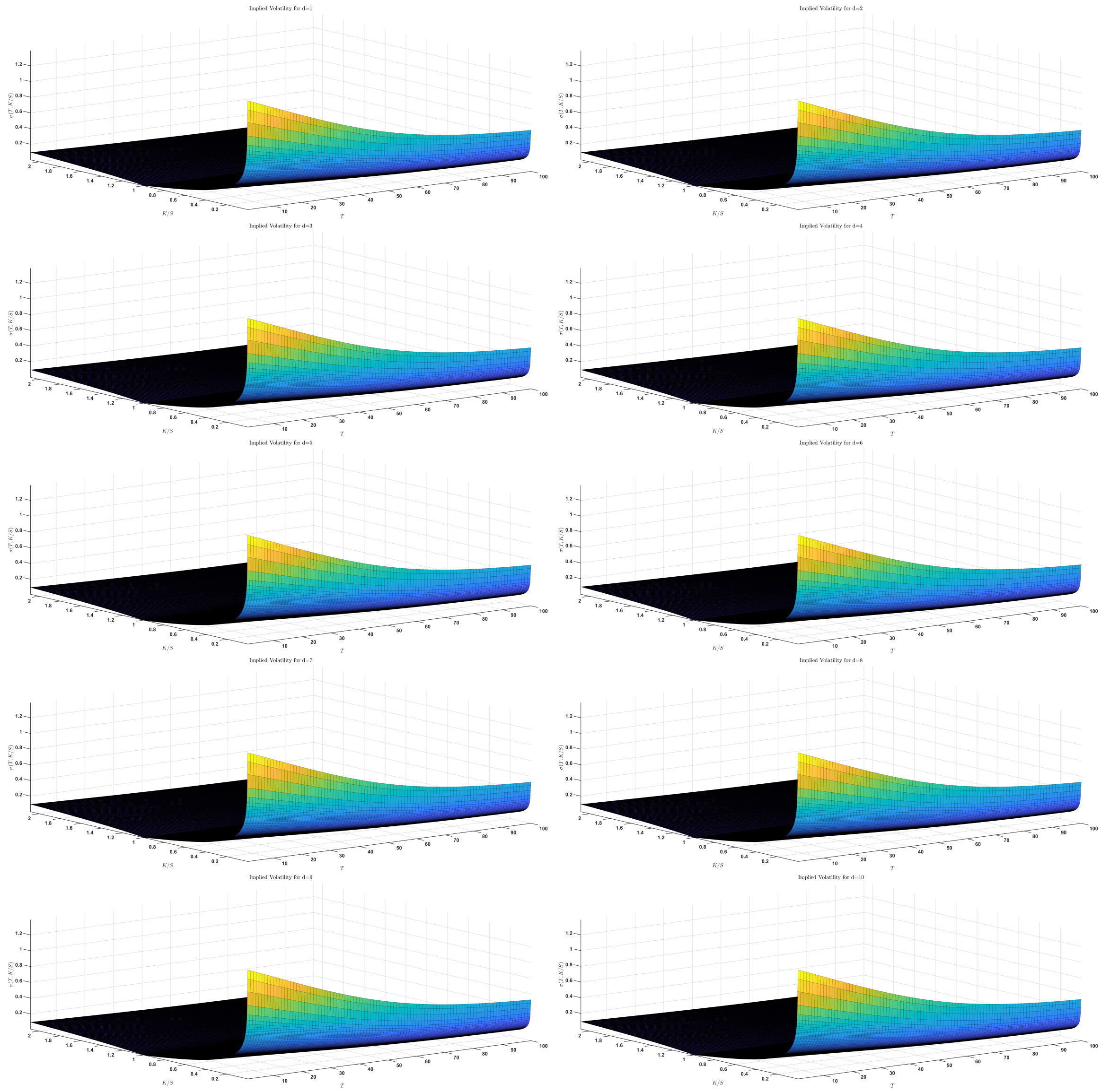

Figure 17: GMP Implied volatility surfaces for depths $1, 2, ..., 10$ for AAPL

Moreover, there is a notable minimum volatility observed close to zero moneyness, particularly evident as moneyness approaches 1 from both in-the-money and out-of-the-money options. This phenomenon suggests that market participants perceive lower risk and uncertainty for options with

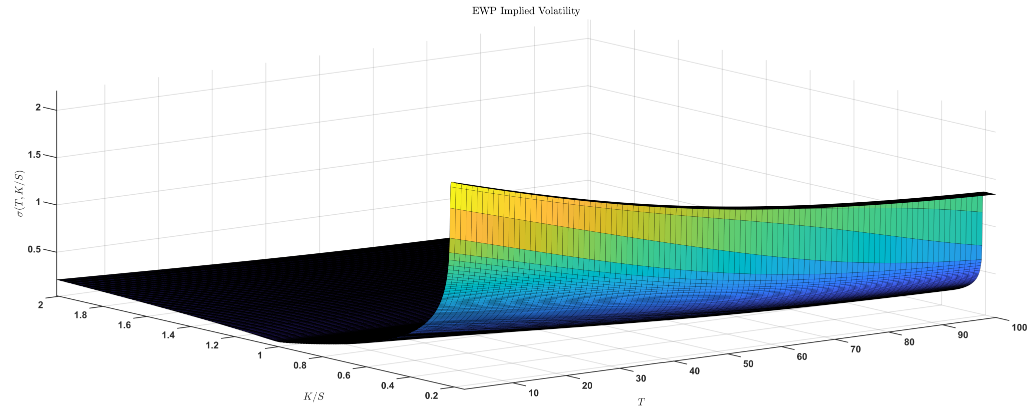

Figure 18: GMP Implied volatility surface for EWP

moneyness near 1, reflecting a more stable pricing environment.

Interestingly, the implied volatility surface for GMP exhibits a consistent shape across different depths, with minimal variation in implied volatility as depth increases. Unlike the TMOBBAS index, where implied volatility decreases with increasing depth, the implied volatility of GMP remains relatively stable across all depths. This uniformity in implied volatility suggests a robust and stable pricing environment for options on the GMP index, regardless of the market depth.

Comparing the implied volatility of the GMP with that of the TMOBBAS across all depths reveals that the implied volatility of the GMP is consistently lower. This disparity in implied volatility underscores the differences in market dynamics and risk perceptions between the two indices, with the GMP exhibiting lower perceived risk and volatility than the TMOBBAS.

Regarding the implied volatility surface of the EWP for the GMP, our analysis indicates that it has a slightly higher volatility than the implied volatility of each depth of GMP. This suggests that while the overall level of volatility may vary, the underlying volatility dynamics captured by the implied volatility surface exhibits uniform characteristics across different depths of the GMP. Also, despite this difference in overall volatility levels, we observe a remarkable similarity in the shapes of the implied volatility surfaces.

Similar to the individual depths of GMP, the implied volatility surface of the EWP also displays the characteristic volatility "smile," with a sharp increase in volatility as the moneyness approaches zero. Additionally, the minimum volatility is observed close to zero moneyness, as the options move both in-the-money and out-of-the-money.

In conclusion, our analysis of the option pricing and implied volatility surfaces for both the TMOBBAS and GMP indices reveals intriguing insights into the dynamics of the market and the behavior of the volatility. While the TMOBBAS index exhibits distinct characteristics in implied volatility across different depths, with a noticeable decrease in volatility as the depth increases, the GMP index has a more uniform implied volatility across different depths. Despite differences in the overall volatility levels, both indices display similar shapes in their implied volatility surfaces, characterized by the volatility "smile." Moreover, the EWP for both indices serves as a comprehensive representation of market sentiment and volatility, aggregating information from diverse depths. Overall, these findings underscore the importance of considering the market depth and composition of the index in understanding and predicting option pricing dynamics and implied volatility in high-frequency trading environments.

7 Evaluation of Risk–Return Performance

In this section, we will focus on measuring the risk–return performance for TMOBBAS and GMP. To do this, we will employ the Rachev ratio (Biglova et al., 2004) as the metric. Unlike *reward-to-variability* ratios such as the well-known Sharpe ratio (Sharpe, 1966) and Sortino ratio (Sortino and Price, 1994), the Rachev ratio is a reward-to-risk ratio designed to assess the potential for extreme positive returns relative to the risk of extreme losses in a non-Gaussian setting. Intuitively, it reflects the potential for significant gains compared to the risk of significant losses, at a rarity frequency q (quantile level) defined by the researcher.

The formula to compute Rachev ratio for the TMOBBAS or GMP is

$$\mathrm{RR}_{(\beta,\gamma)}(X) := \frac{\mathrm{AVaR}_{\beta}(-X)}{\mathrm{AVaR}_{\gamma}(X)} \tag{14}$$

where

- X denotes the log-return of TMOBBAS or GMP at a given time interval.
- $\mathrm{AVaR}_{\gamma}(X) := \gamma^{-1}\int_0^{\gamma}\mathrm{VaR}_u(X)\,\mathrm{d}u$ is the average Value-at-Risk (VaR) at the level $\gamma \in (0,1]$.
- $\mathrm{VaR}_u(X) := \inf\{m \in \mathbb{R} : \mathbb{P}[X+m<0] \le u\}$ is the VaR at the level u.

The formula to compute $\mathrm{AVaR}_{\gamma}(X)$ may seem a bit challenging. However, according to (Föllmer and Schied, 2004), we know that

$$\mathrm{AVaR}_{\beta}(X) = \frac{\mathbb{E}[(q-X)^{+}]}{\beta} - q \tag{15}$$

where

- q is the β-quantile of X
- $(q-X)^{+} := \max(q-X, 0)$.

In this study, we set $\beta = \gamma = 0.05$ to explore the relationship between excess profit and excess loss when "investing" in the TMOBBAS. Next, we merge Equation (14) and Equation (15), applying them to our dataset for AMZN, AAPL, and GOOG. Figure 19 illustrates the evolution of the Rachev ratio of TMOBBAS and GMP for AMZN, AAPL, and GOOG across different depths.

From Figure 19a, we can observe that

- The general trend shows that as the depth increases, the Rachev ratio initially rises and then declines.
- For AAPL, the Rachev ratio remains consistently above 1 across different depths, suggesting that excess losses can always be offset by excess profits when investing in TMOBBAS at varying depths of AAPL. In particular, the highest Rachev ratio occurs at a depth of 2.
- In the case of AMZN, as the depth increases to 5 or beyond, the Rachev ratio drops below 1, indicating that excess losses cannot be balanced by excess profits when investing in TMOBBAS at such depths. Similarly to AAPL, the Rachev ratio for AMZN peaks at a depth of 2.
- For GOOG, as the depth increases to 6 or beyond, the Rachev ratio falls below 1, suggesting that excess losses cannot be balanced by excess profits when investing in TMOBBAS at such depths. Notably, the Rachev ratio for GOOG achieves relatively high values at depths 2 and 3.

From Figure 19b, we can observe that

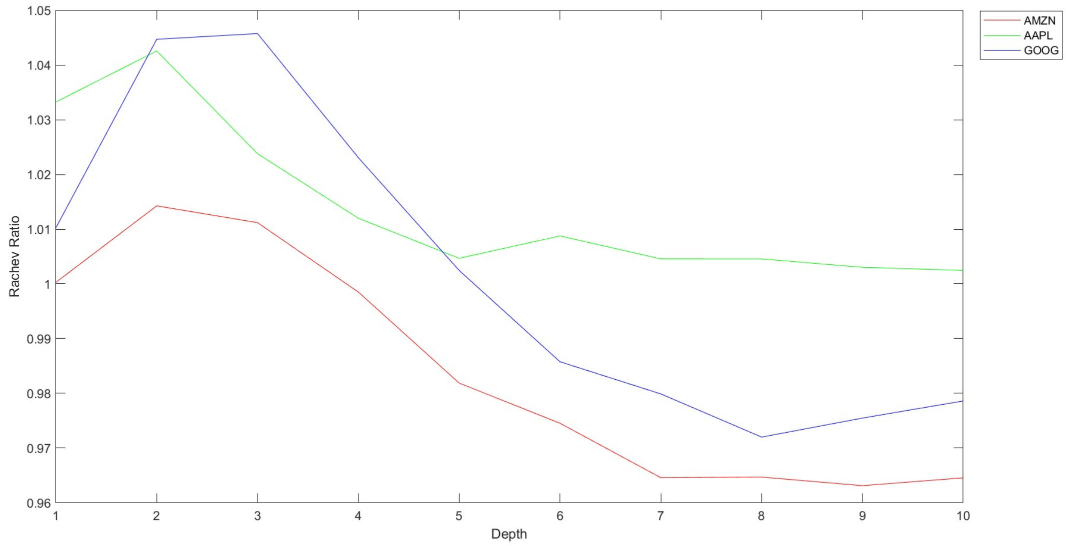

(a)

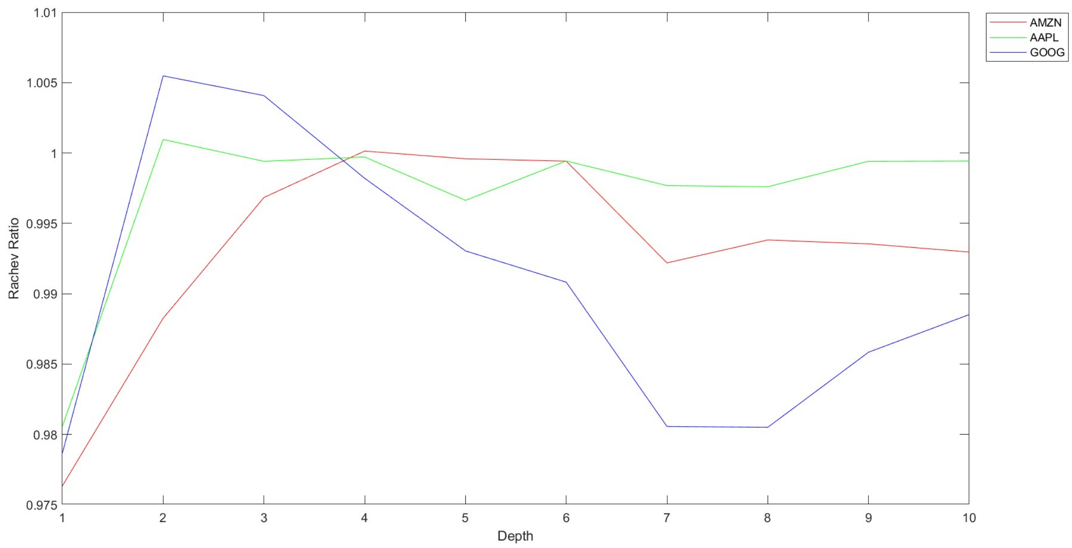

(b)

Figure 19: The evolution of Rachev ratio of (a) TMOBBAS and (b) GMP for AMZN, AAPL, and GOOG over depth (AMZN, AAPL, and GOOG represented by red, green, and blue line, respectively)

- The general trend shows that as the depth increases, the Rachev ratio initially rises and then declines.
- For AAPL, the Rachev ratio increases first, reaching its peak at a depth of 2, approximately 1.001. Then, this value remains close to, but less than, 1 for the next eight depths. This suggests that the excess loss can almost be balanced by the excess profit when investing in GMP for AAPL at various depths.
- For AMZN, the Rachev ratio also increases initially, reaching its peak at a depth of 4, around 1. Afterward, the overall trend of the Rachev ratio is to decrease until it reaches a value of approximately 0.993 at a depth of 10. This suggests that the excess loss cannot almost be balanced by the excess profit when investing GMP for AMZN at various depths.
- For GOOG, the Rachev ratio initially increases, reaching its peak at a depth of 2, approximately 1.005. It then decreases to its lowest point at a depth of 8, around 0.981, before increasing again to about 0.988 at a depth of 10. Overall, we can see that the excess loss can be balanced by the excess profit when investing in GMP for GOOG at depths of 2, 3, and 4. However, for other depths, the excess loss cannot be balanced by excess profit.

8 Summary

This paper has ventured beyond traditional analyses of limit order books (LOBs) to introduce and scrutinize two pivotal concepts: the total market order book bid–ask spread (TMOBBAS) and the global mid-price (GMP). Our exploration, grounded in high-frequency data, achieves nuanced understandings of market liquidity, volatility, and efficiency through the lens of these novel metrics. The study highlights the significance of considering the entire depth of the LOB in capturing the complexity of market dynamics, a perspective that enriches our comprehension of financial markets in the era of high-frequency trading.

Our findings underscore the multifaceted nature of the TMOBBAS and GMP, illustrating their roles in offering strategic insights into the prediction of spreads and understanding the behavior of the market. By examining the analysis of the tail behavior, the dynamics of the log-returns, and risk–return performance, we have provided a comprehensive assessment of the risks and returns associated with these measures under different market conditions.

The implications of our study are many, touching upon practical aspects for traders and risk managers, as well as theoretical contributions to financial market research. Our analysis not only advances the academic discourse by introducing innovative concepts in the study of LOBs but also offers valuable insights for market participants navigating the complexities of modern financial systems. In doing so, this paper bridges the gap between theoretical models and practical realities, paving the way for future research and strategic applications in financial market analysis.

Data Availability Statement

Publicly available datasets were analyzed in this study. This data can be found here: LOBSTER (`https://lobsterdata.com/`).

Author Contributions

YH: Data curation, Formal analysis, Investigation, Methodology, Software, Validation, Visualization, Writing - original draft, Writing - review & editing; AS: Data curation, Formal analysis, Methodology, Software, Validation, Writing - original draft, Writing - review & editing; BS: Writing

- review & editing; SR: Conceptualization, Investigation, Methodology, Project administration, Resources, Supervision, Visualization, Writing - review & editing; FF: Resources, Writing - review & editing

Disclosure Statement

The authors declare that the research was conducted in the absence of any commercial or financial relationships that could be constructed as a potential conflict of interest.

Funding

The authors declare that no financial support was received for the research, authorship, and publication of this article.

References

Abergel, F., Anane, M., Chakraborti, A., Jedidi, A., and Toke, I. M. (2016). *Limit Order Books*. Cambridge University Press.

Balkema, A. A. and De Haan, L. (1974). Residual life time at great age. *The Annals of Probability*, 2(5):792–804.

Biglova, A., Ortobelli, S., Rachev, S. T., and Stoyanov, S. (2004). Different approaches to risk estimation in portfolio theory. *The Journal of Portfolio Management*, 31(1):103–112.

Bollerslev, T. (1986). Generalized autoregressive conditional heteroskedasticity. *Journal of Econometrics*, 31(3):307–327.

Brogaard, J., Hendershott, T., and Riordan, R. (2014). High-frequency trading and price discovery. *The Review of Financial Studies*, 27(8):2267–2306.

Carr, P. and Madan, D. (1998). Option valuation using the fast Fourier transform. *Journal of Computational Finance*, 2:61–73.

Clark, P. (1973). A subordinated stochastic process model with fixed variance for speculative prices. *Econometrica*, 41:135–156.

Cont, R. (2001). Empirical properties of asset returns: Stylized facts and statistical issues. *Quantitative Finance*, 1(2):223.

Davison, A. C. (1984). Modelling excesses over high thresholds, with an application. In *Statistical Extremes and Applications*, pages 461–482. Springer-Verlag.

De Haan, L. and Peng, L. (1998). Comparison of tail index estimators. *Statistica Neerlandica*, 52(1):60–70.

Duffie, D. (2010). *Dynamic Asset Pricing Theory*. Princeton University Press.

Eagle, R. F. (1982). Autoregressive conditional heteroskedasticity with estimates of the variance of UK inflation. *Econometrica*, 50(4):987–1007.

Embrechts, P., Mikosch, T., and Klüppelberg, C. (1997). *Modelling Extremal Events: For Insurance and Finance*. Springer-Verlag.

Föllmer, H. and Schied, A. (2004). *Stochastic Finance: An Introduction in Discrete Time*. Walter de Gruyter.

Gould, M. D., Porter, M. A., Williams, S., McDonald, M., Fenn, D. J., and Howison, S. D. (2013). Limit order books. *Quantitative Finance*, 13(11):1709–1742.

Grimshaw, S. D. (1993). Computing maximum likelihood estimates for the generalized Pareto distribution. *Technometrics*, 35(2):185–191.

Haeusler, E. and Segers, J. (2007). Assessing confidence intervals for the tail index by Edgeworth expansions for the Hill estimator.

Hill, B. M. (1975). A simple general approach to inference about the tail of a distribution. *The Annals of Statistics*, pages 1163–1174.

Hogg, R. V. (1972). More light on the kurtosis and related statistics. *Journal of the American Statistical Association*, 67(338):422–424.

Hogg, R. V. (1974). Adaptive robust procedures: A partial review and some suggestions for future applications and theory. *Journal of the American Statistical Association*, 69(348):909–923.

Hosking, J. R. and Wallis, J. R. (1987). Parameter and quantile estimation for the generalized Pareto distribution. *Technometrics*, 29(3):339–349.

Huang, R. and Polak, T. (2011). LOBSTER: Limit Order Book Rreconstruction System. *Available at SSRN 1977207*.

Lundtofte, F. and Wilhelmsson, A. (2013). Risk premia: Exact solutions vs. log-linear approximations. *Journal of Banking & Finance*, 37:4256–4264.

Lux, T. (2009). Stochastic behavioral asset-pricing models and the stylized facts. In *Handbook of Financial Markets: Dynamics and Evolution*, pages 161–215. Elsevier.

Mandelbrot, B. B. and Taylor, H. M. (1967). On the distribution of stock price differences. *Journal of Operations Research*, 15:1057–1062.

McNeil, A. J., Frey, R., and Embrechts, P. (2015). *Quantitative Risk Management: Concepts, Techniques and Tools—Revised Edition*. Princeton University Press.

O'Hara, M. (1998). *Market Microstructure Theory*. Wiley.

Paulson, A. S., Holcomb, E. W., and Leitch, R. A. (1975). The estimation of the parameters of the stable laws. *Biometrika*, 62:163–170.

Pickands III, J. (1975). Statistical inference using extreme order statistics. *the Annals of Statistics*, pages 119–131.

Rachev, S. T. and Mittnik, S. (2000). *Stable Paretian Models in Finance*. Wiley.

Rogers, L. C. G. and Zhang, L. (2011). An asset return model capturing stylized facts. *Mathematics and Financial Economics*, 5(2):101–119.

Sato, K.-I. (1999). *Lévy Processes and Infinitely Divisible Distributions*. Cambridge University Press.

Schoutens, W. (2003). *Lévy Processes in Finance: Pricing Financial Derivatives*. Wiley, Hoboken, NJ.

Sharpe, W. F. (1966). Mutual fund performance. *The Journal of Business*, 39(1):119–138.

Shimokawa, T., Suzuki, K., and Misawa, T. (2007). An agent-based approach to financial stylized facts. *Physica A: Statistical Mechanics and its Applications*, 379(1):207–225.

Shirvani, A., Mittnik, S., Lindquist, W. B., and Rachev, S. T. (2023). Bitcoin volatility and intrinsic time using double subordinated levy processes.

Shirvani, A., Rachev, S. T., and Fabozzi, F. J. (2021a). Multiple subordinated modeling of asset returns: Implications for option pricing. *Econometric Reviews*, 40(3):290–319.

Shirvani, A., Stoyanov, S. V., Fabozzi, F. J., and Rachev, S. T. (2021b). Equity premium puzzle or faulty economic modelling? *Review of Quantitative Finance and Accounting*, 56:1329–1342.

Shreve, S. E. (2004). *Stochastic Calculus for Finance II: Continuous-Time Models*. Springer-Verlag.

Smith, R. L. (1985). Maximum likelihood estimation in a class of nonregular cases. *Biometrika*, 72(1):67–90.

Smith, R. L. (1987). Estimating tails of probability distributions. *The Annals of Statistics*, pages 1174–1207.

Sortino, F. A. and Price, L. N. (1994). Performance measurement in a downside risk framework. *The Journal of Investing*, 3(3):59–64.

Tsay, R. S. (2005). *Analysis of Financial Time Series*. Wiley.

Yao, L., Yang, G., and Yang, X. (2011). A note on the mean correcting martingale measure for geometric Lévy processes. *Applied Mathematics Letters*, 24(5):593–597.

Yu, J. (2003). Empirical characteristic function estimation and its applications. *Econometric Reviews*, 23:93–123.

A Figures for AMZN

A.1 Static Method

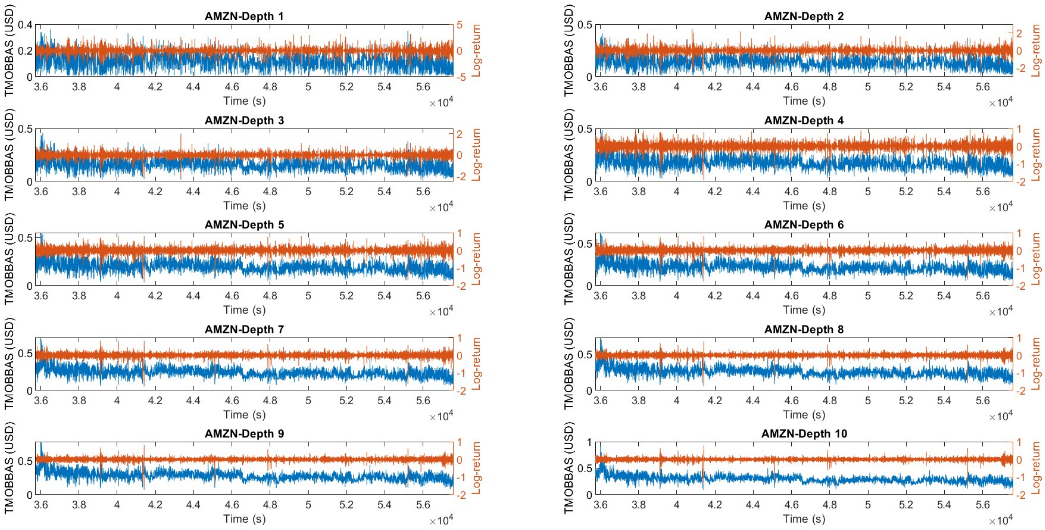

(a)

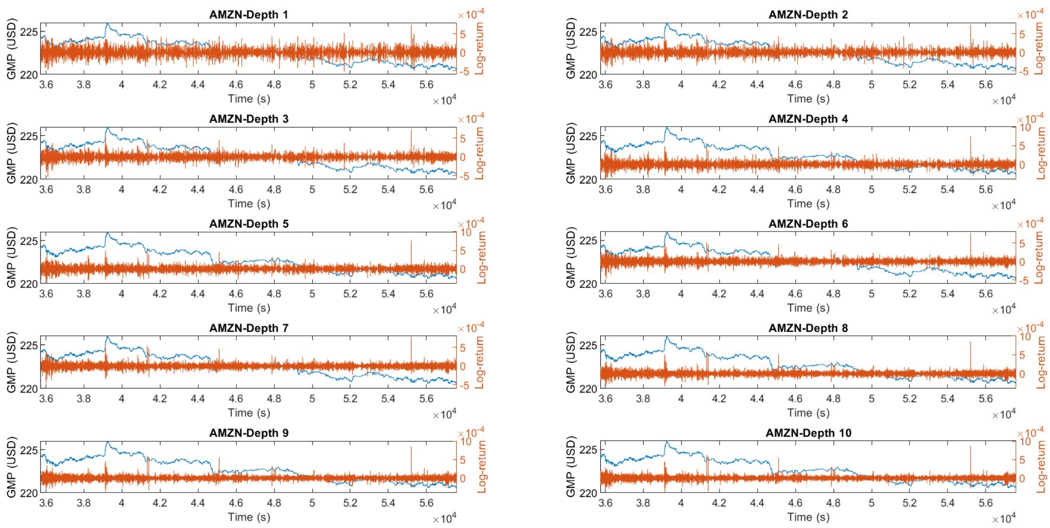

(b)

Figure 20: The evolution of (a) TMOBBAS, (b) GMP and their log-returns over time at all 10 different depths for AMZN (Each graph contains two y-axes. The left y-axis is for TMOBBAS (or GMP), and the right y-axis is for the log-return. The evolution of TMOBBAS (or GMP) is represented by the blue line while the evolution of the log-returns is represented by the orange line.)

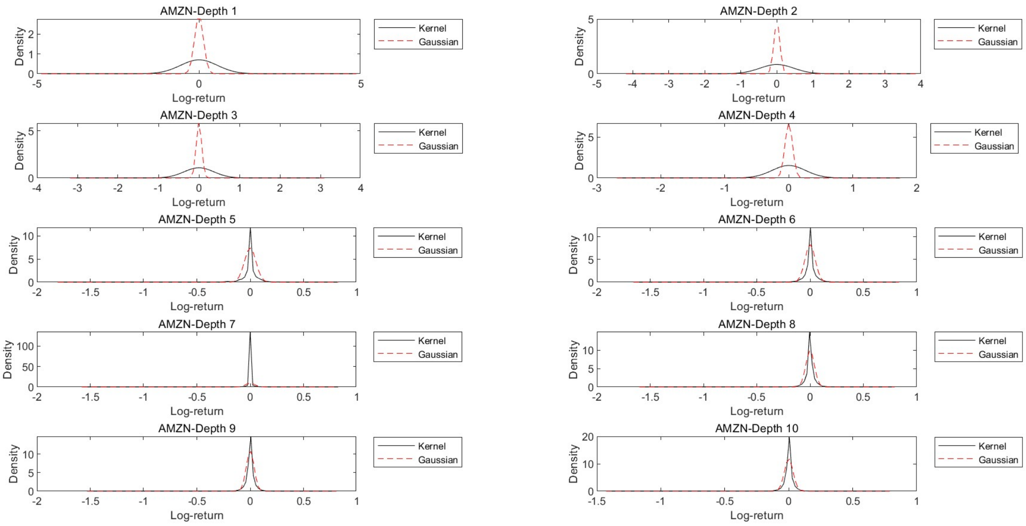

(a)

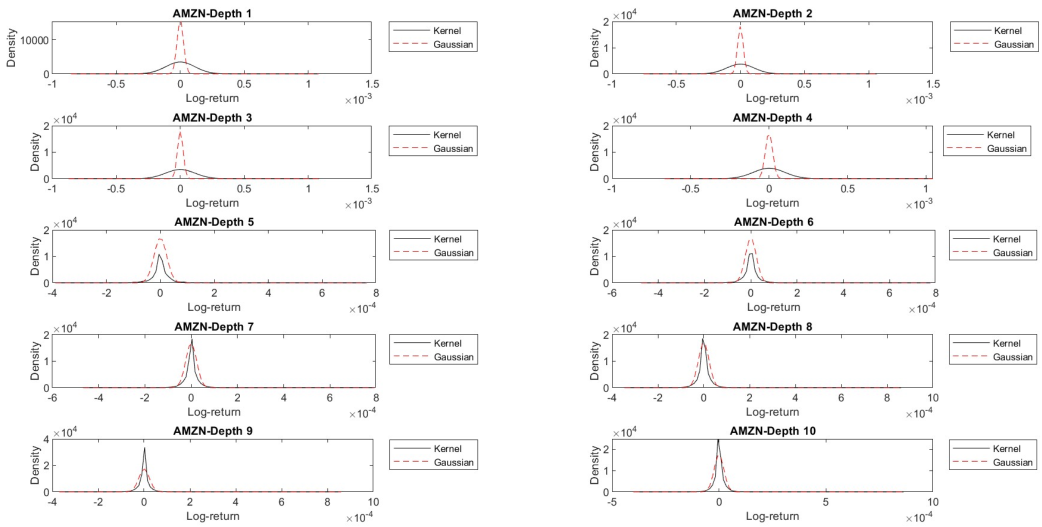

(b)

Figure 21: Comparison of the kernel density (represented by black solid lines) of log-returns of (a) TMOBBAS, (b) GMP with the corresponding Gaussian distribution with the same sample mean and standard deviation (depicted by the red dashed lines) at all 10 depths for AMZN

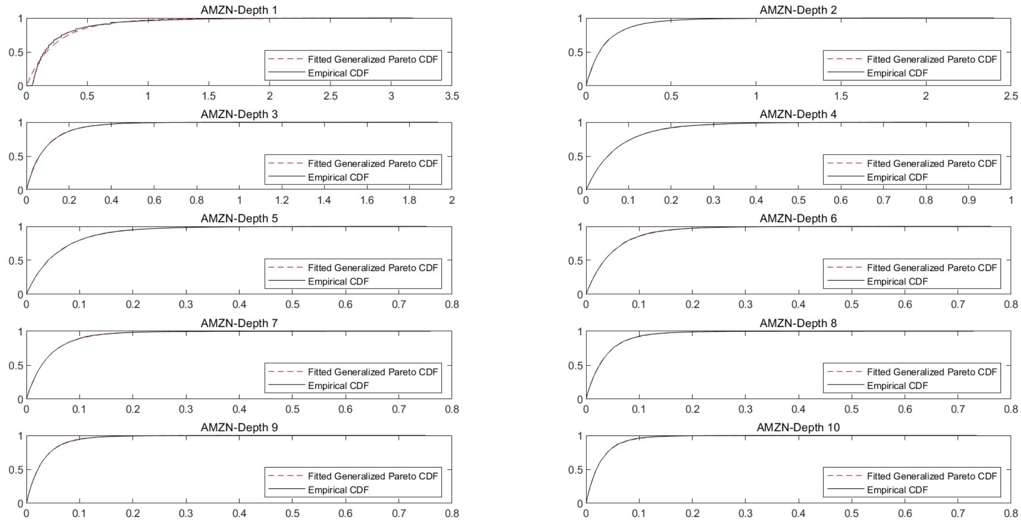

(a)

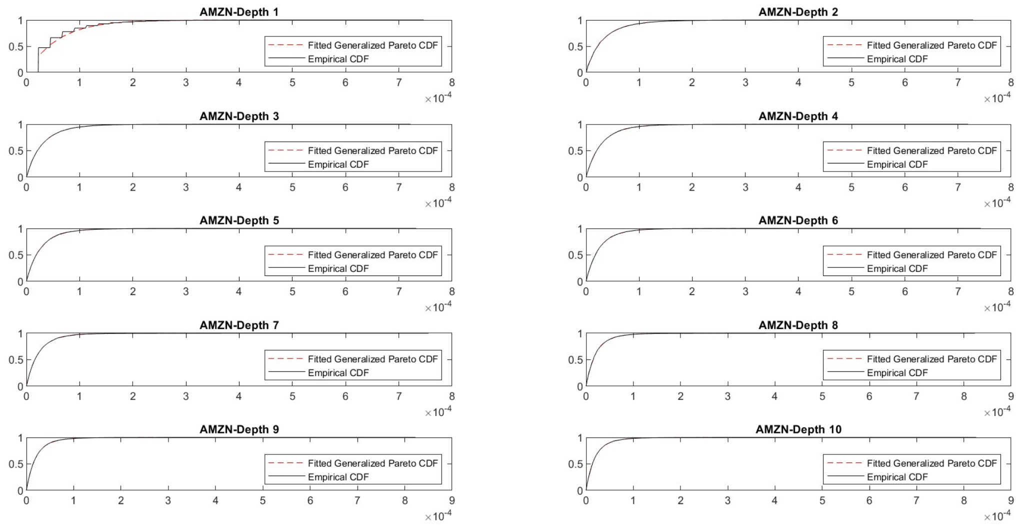

(b)

Figure 22: Comparison of empirical CDF (represented by black solid lines) of tail and its fitted CDF of GPD of (a) TMOBBAS and (b) GMP at all 10 depths for AMZN

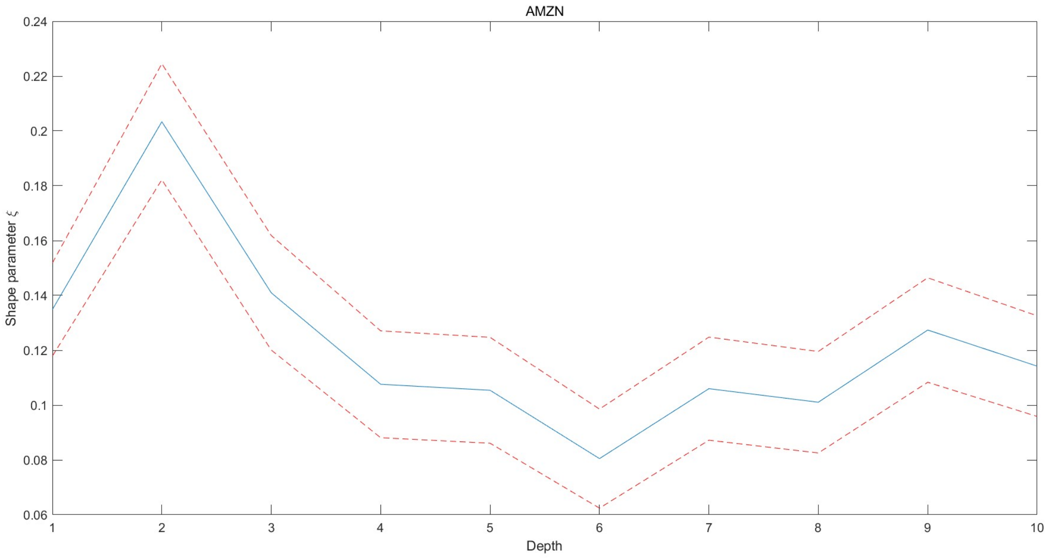

(a)

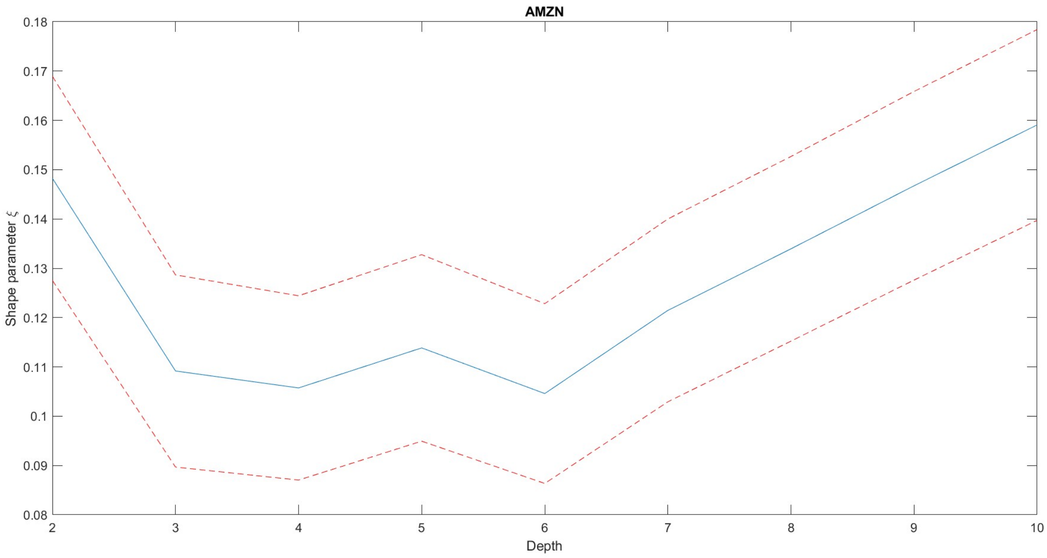

(b)

Figure 23: The evolution of estimated shape parameter ξ (represented by blue solid line) and its corresponding 95% CI (depicted by two red dashed lines) for (a) TMOBBAS and (b) GMP over depth for AMZN

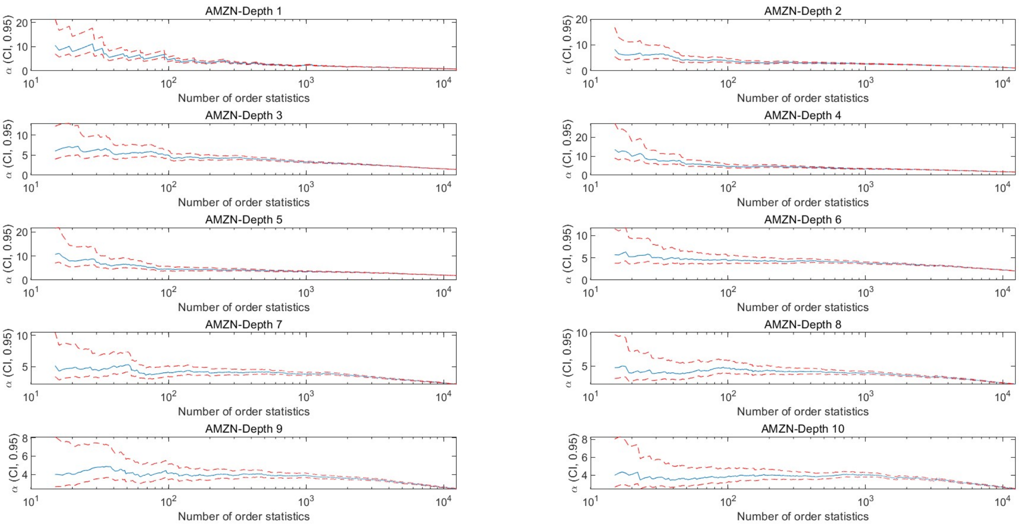

(a)

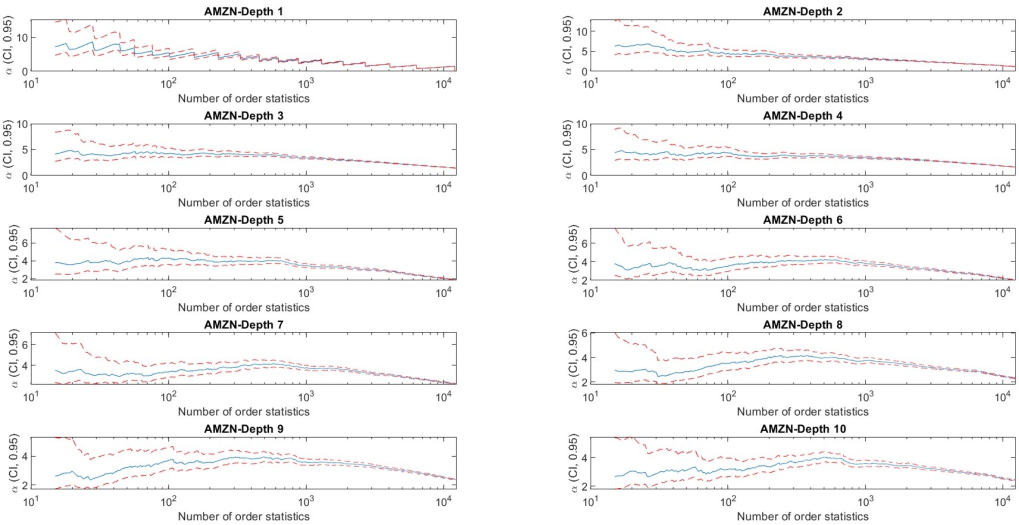

(b)

Figure 24: The dependence of estimated tail index α (represented by blue solid line) and its corresponding 95% CI (depicted by two red dashed lines) for (a) TMOBBAS and (b) GMP on the number of order statistics at all 10 depths for AMZN

A.2 Dynamic Method

A.2.1 Figures for TMOBBAS

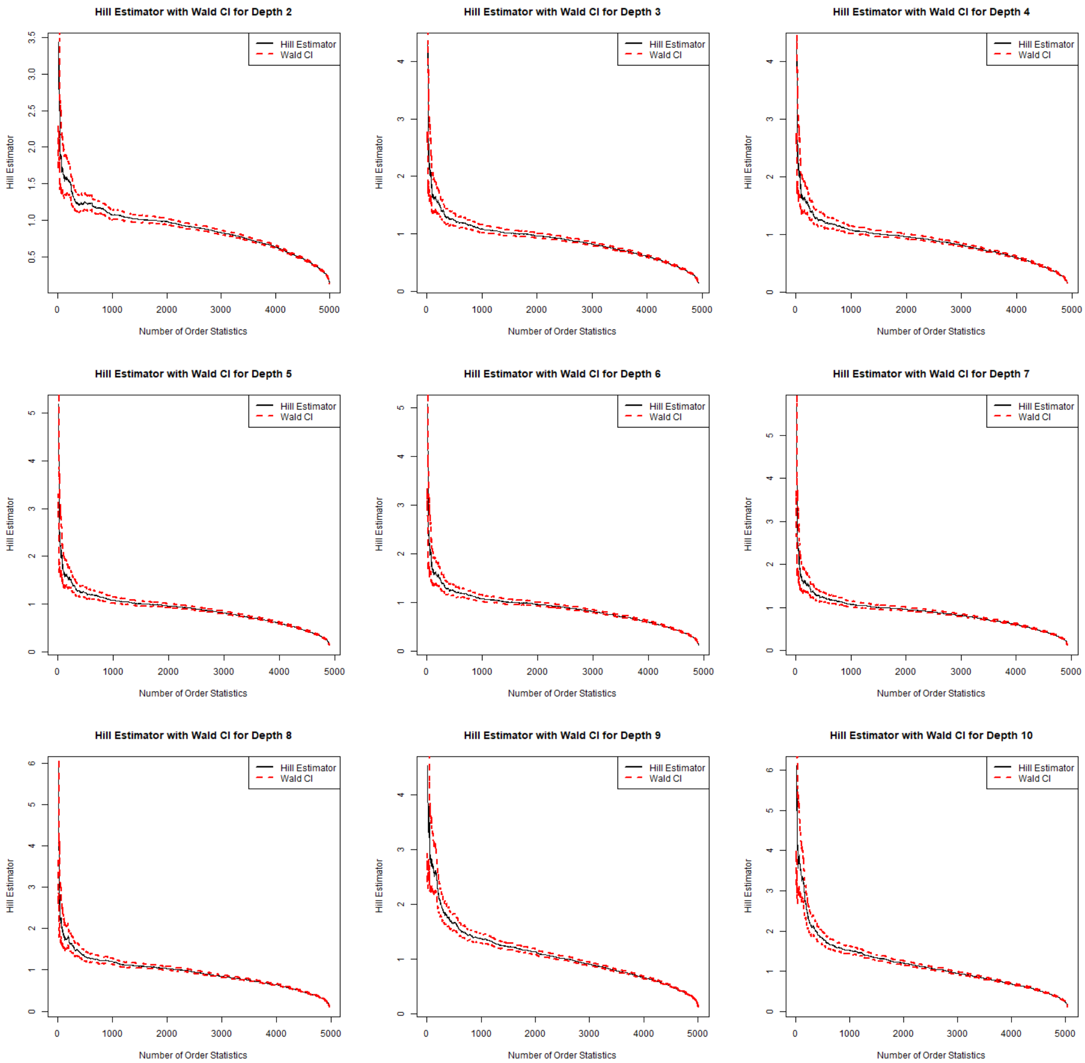

Figure 25: The dependence of estimated tail index α (represented by black solid lines) and its corresponding 95% CI (depicted by two red dashed lines) on the number of order statistics at depths 2, 3, $\cdots$ 10 for AMZN

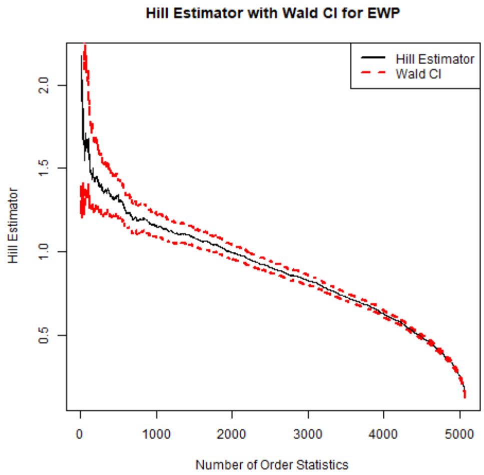

Figure 26: The dependence of estimated tail index α (represented by black solid line) and its corresponding 95% CI (depicted by two red dashed lines) on the number of order statistics for EWP for AMZN

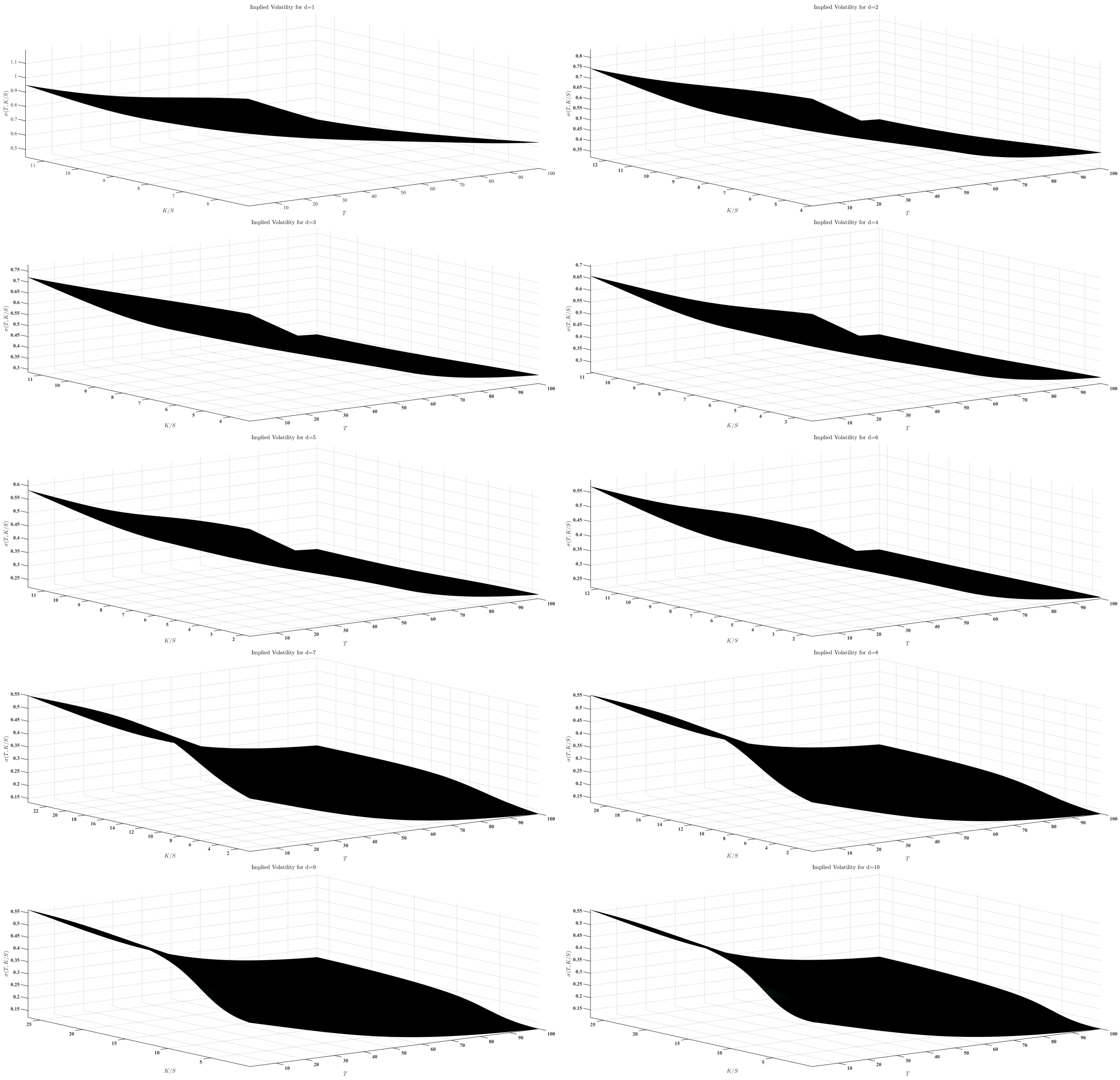

Figure 27: TMOBBAS Implied volatility surfaces for depths $1, 2, ..., 10$ for AMZN

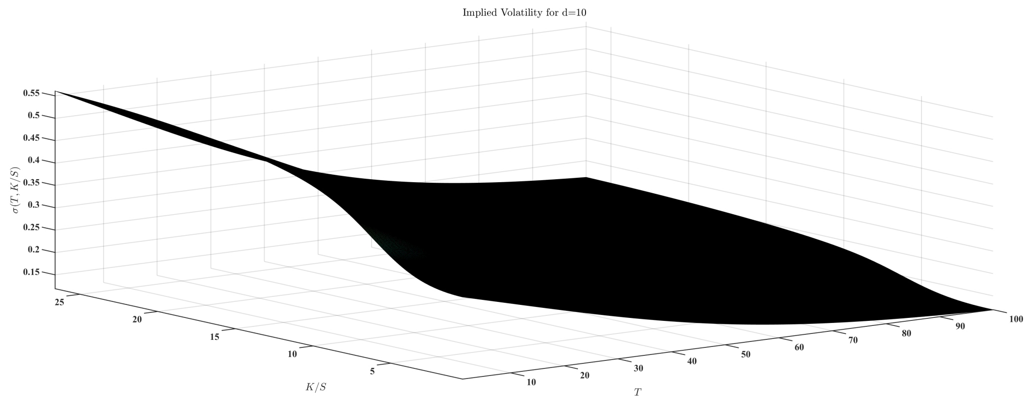

Figure 28: TMOBBAS Implied volatility surface for EWP

A.2.2 Figures for GMP

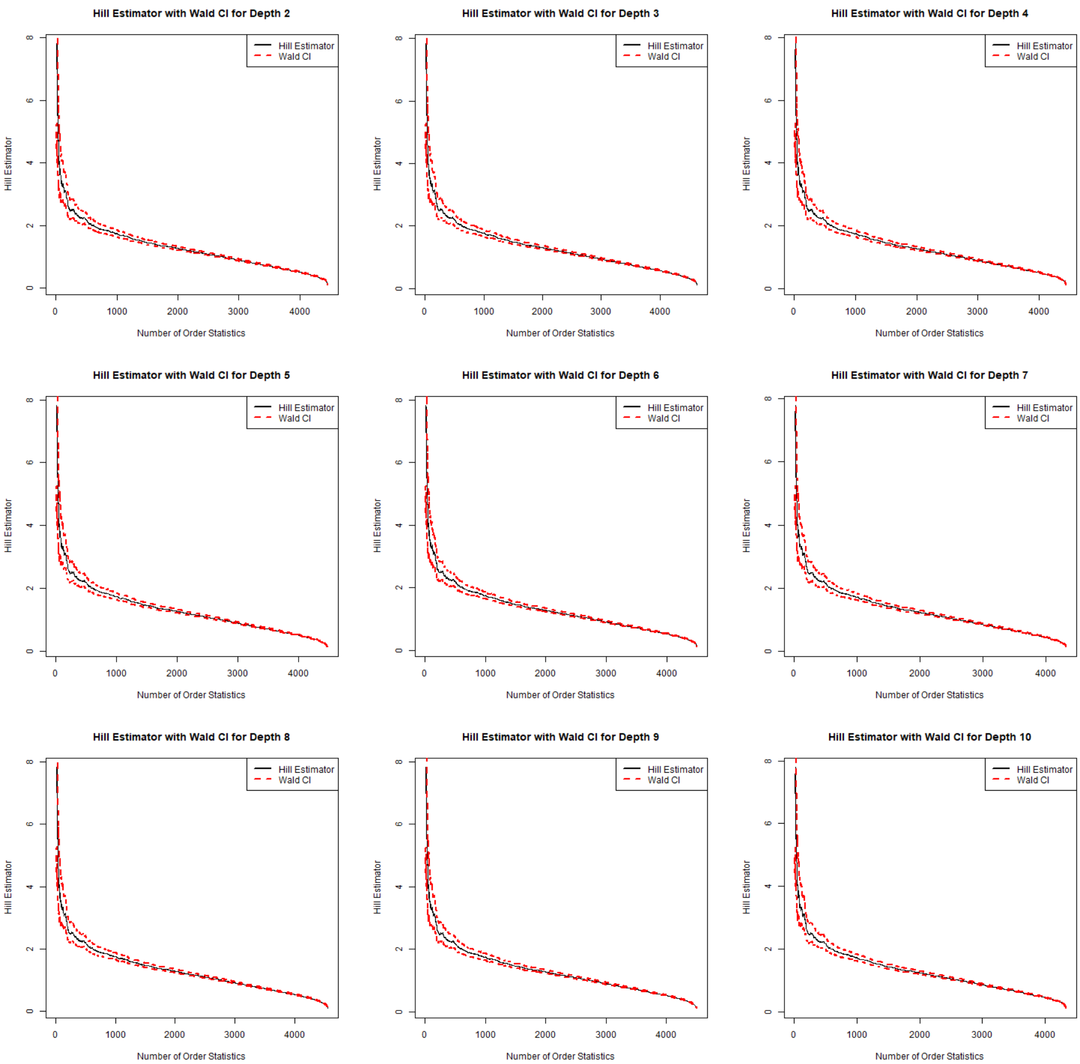

Figure 29: The dependence of estimated tail index α (represented by black solid lines) for GMP and its corresponding 95% CI (depicted by two red dashed lines) on the number of order statistics at depths 2, 3, $\cdots$ 10 for AMZN

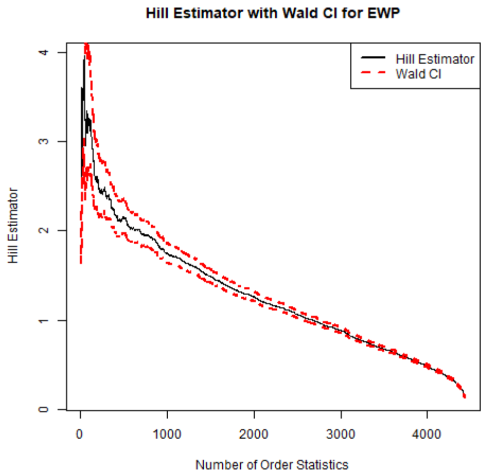

Figure 30: The dependence of estimated tail index α (represented by black solid line) of GMP and its corresponding 95% CI (depicted by two red dashed lines) on the number of order statistics for EWP for AMZN

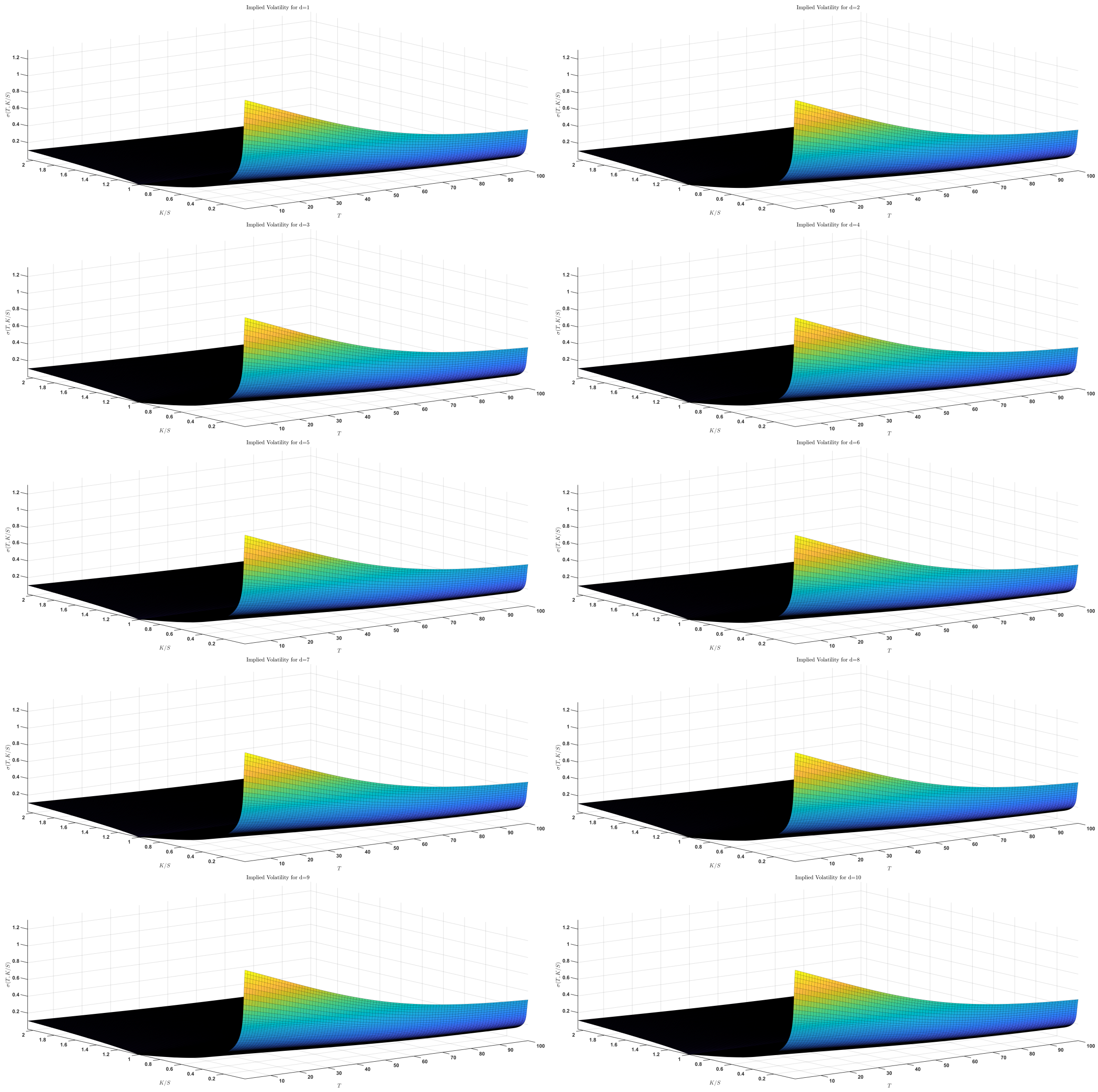

Figure 31: GMP Implied volatility surfaces for depths $1, 2, ..., 10$ for AMZN

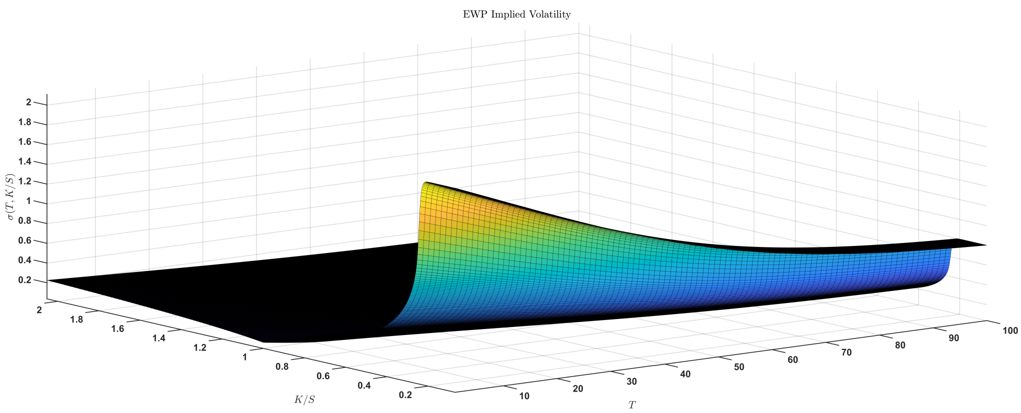

Figure 32: GMP Implied volatility surface for EWP

B Figures for GOOG

B.1 Static Method

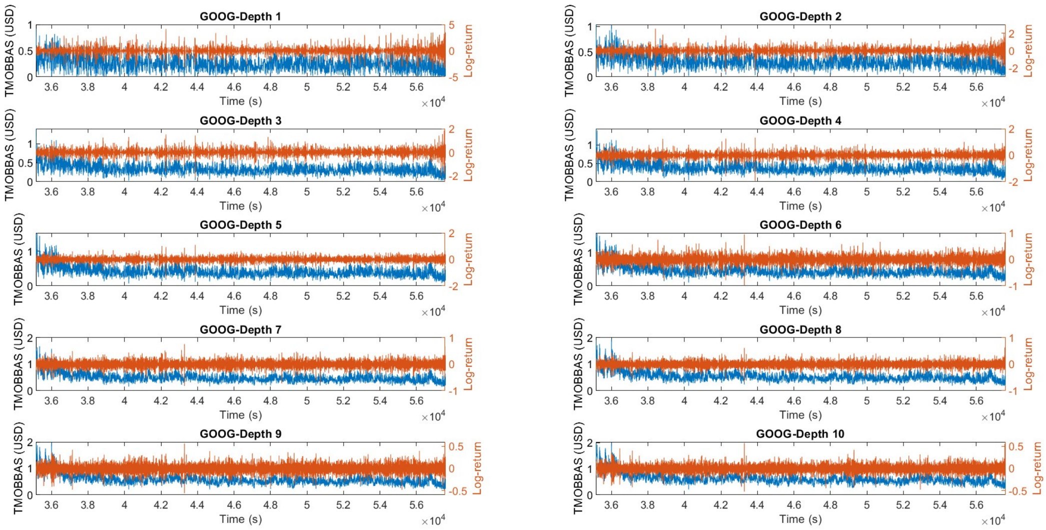

(a)

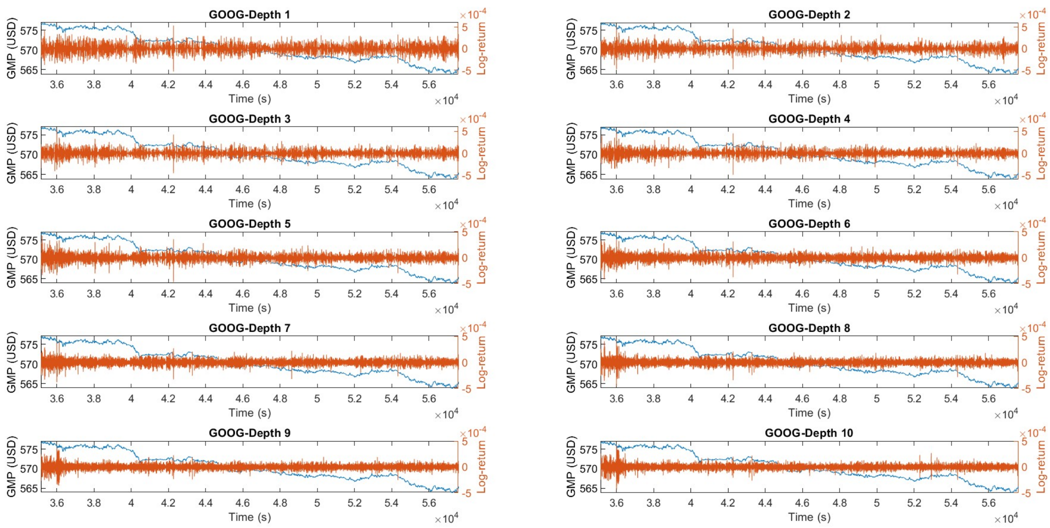

(b)

Figure 33: The evolution of (a) TMOBBAS, (b) GMP and their log-returns over time at all 10 different depths for GOOG (Each graph contains two y-axes. The left y-axis is for the TMOBBAS (or GMP), and the right y-axis is for the log-returns. The evolution of TMOBBAS (or GMP) is represented by a blue line while the evolution of the log-returns is represented by an orange line.)

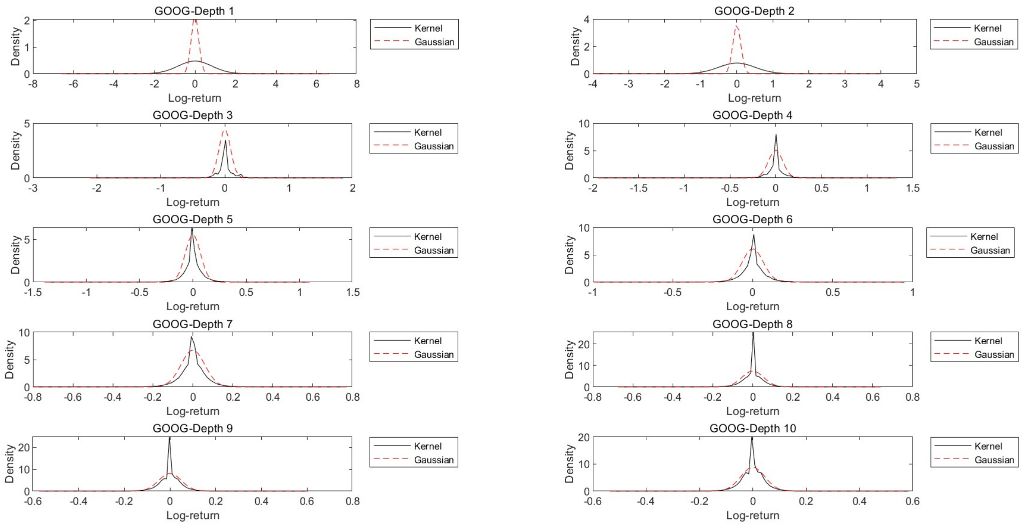

(a)

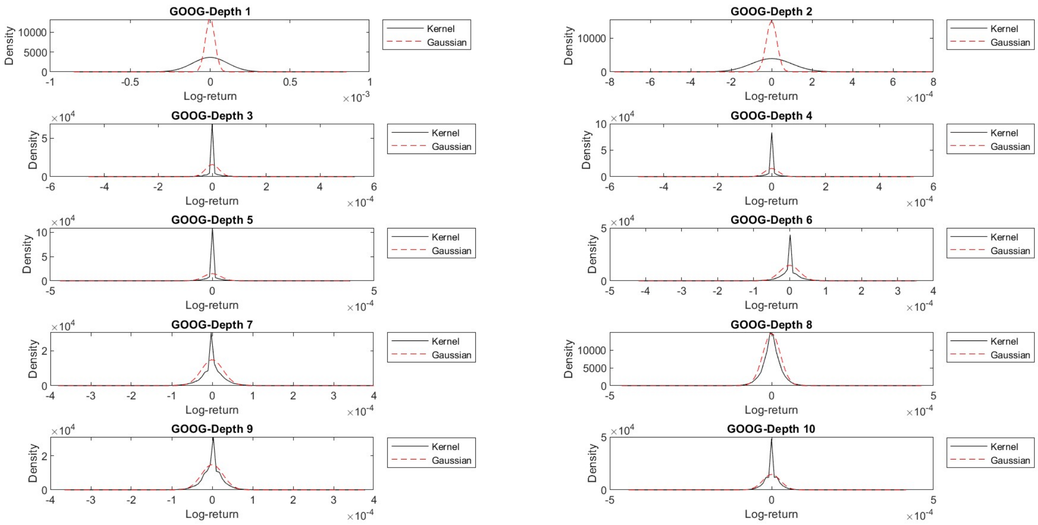

(b)

Figure 34: Comparison of the kernel density (represented by black solid lines) of log-returns of (a) TMOBBAS, (b) GMP and the corresponding Gaussian distribution with the same sample mean and standard deviation (depicted by the red dashed lines) at all 10 depths for GOOG

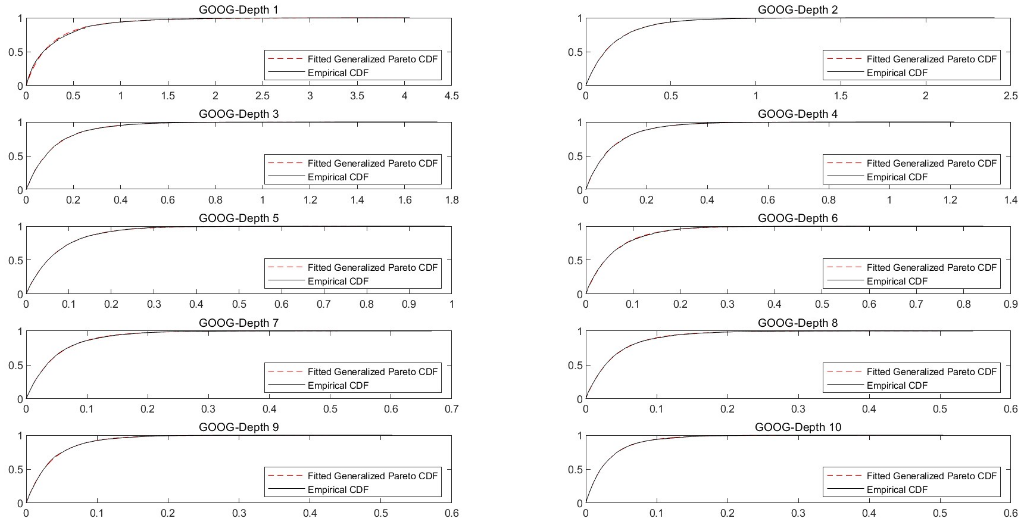

(a)

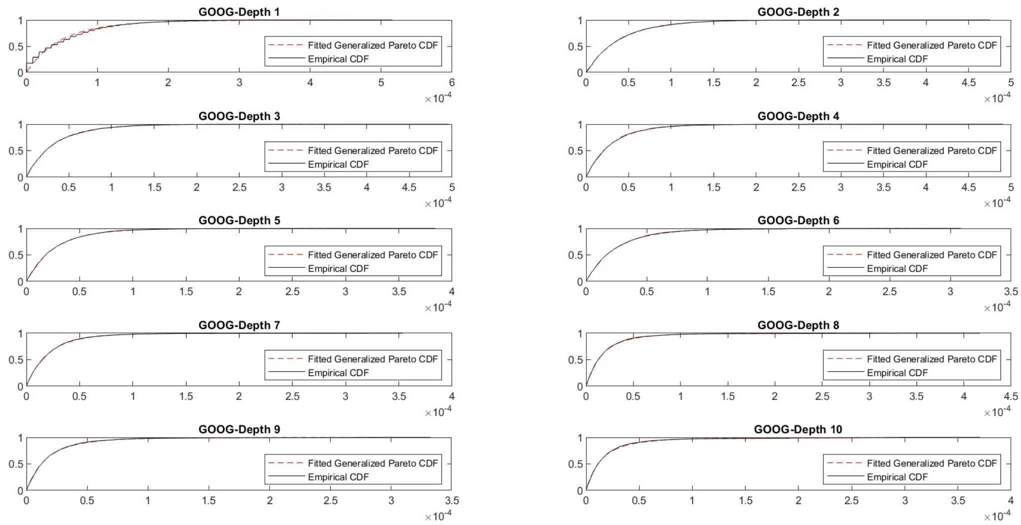

(b)

Figure 35: Comparison of empirical CDF (represented by black solid lines) of tail and its fitted CDF of GPD of (a) TMOBBAS and (b) GMP at all 10 depths for GOOG

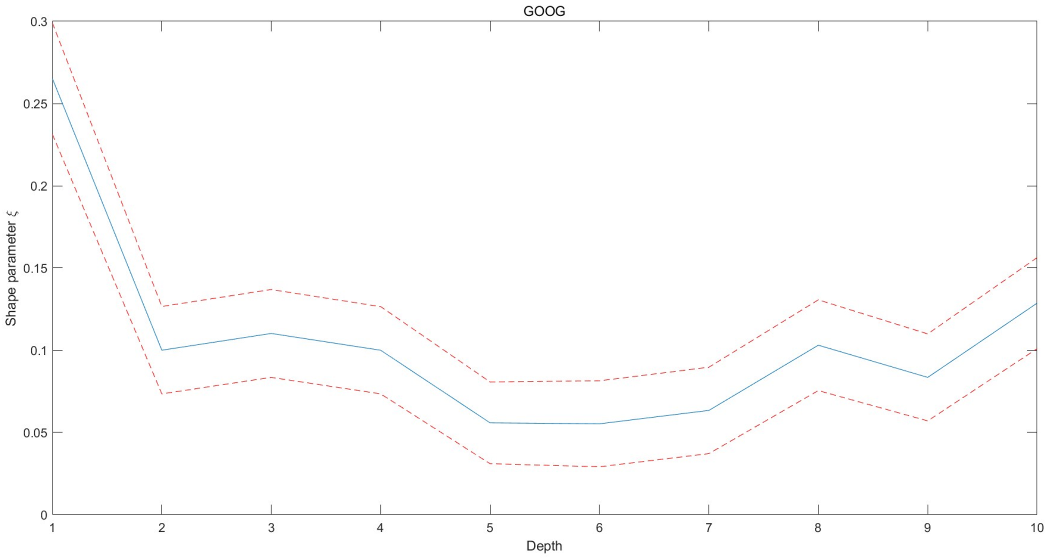

(a)

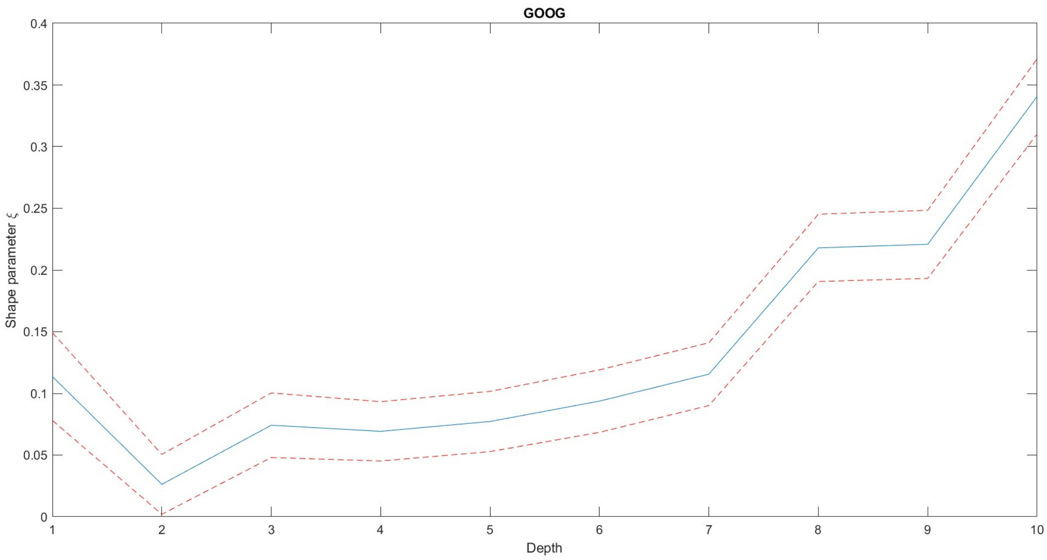

(b)

Figure 36: The evolution of estimated shape parameter ξ (represented by blue solid line) and its corresponding 95% CI (depicted by two red dashed lines) for (a) TMOBBAS and (b) GMP over depth for GOOG

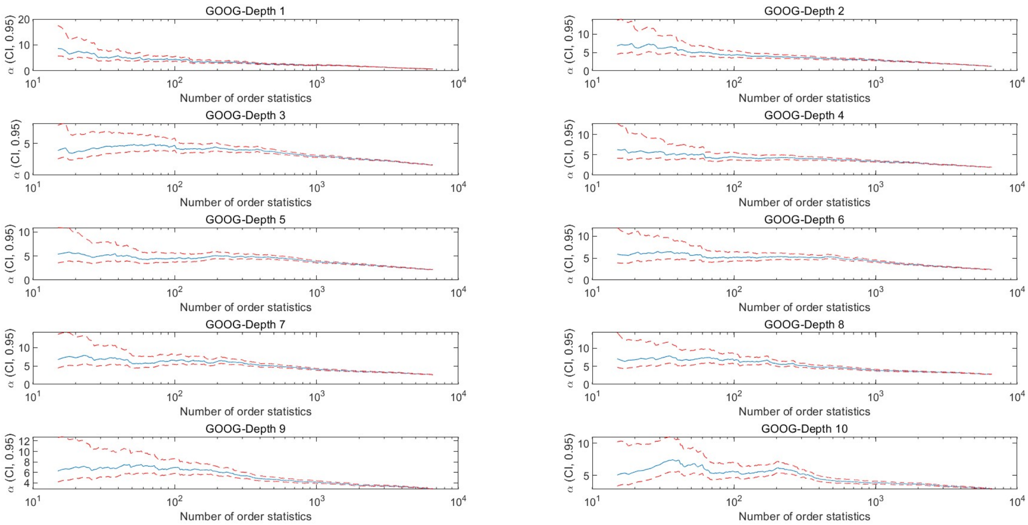

(a)

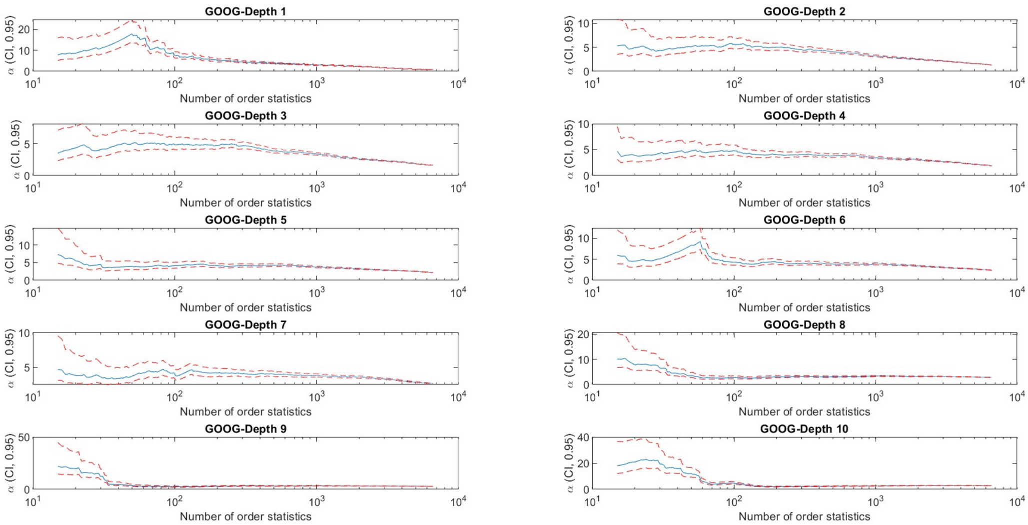

(b)

Figure 37: The dependence of estimated tail index α (represented by blue solid line) and its corresponding 95% CI (depicted by two red dashed lines) for (a) TMOBBAS and (b) GMP on the number of order statistics at all 10 depths for GOOG

B.2 Dynamic Method

B.2.1 Figures for TMOBBAS

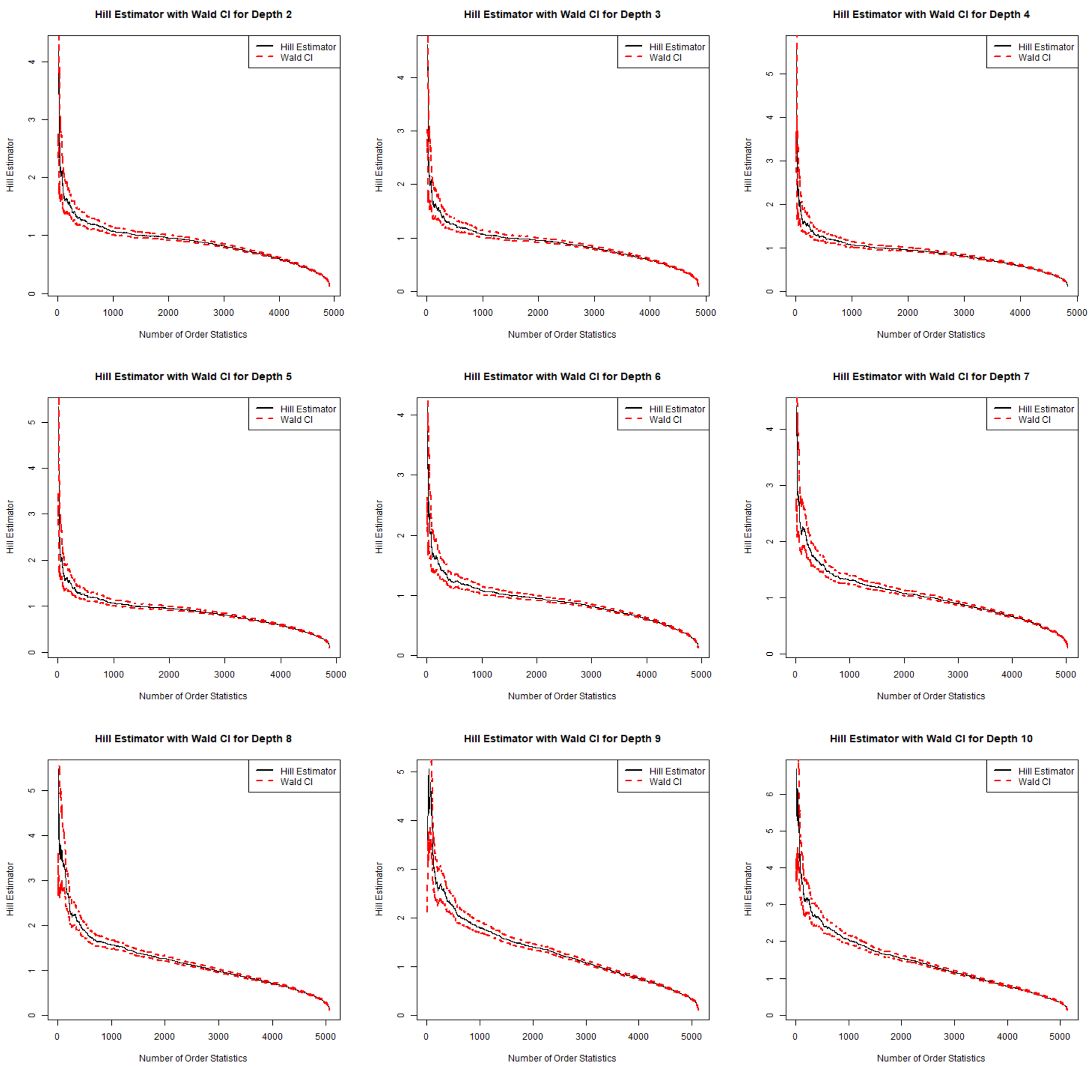

Figure 38: The dependence of estimated tail index α (represented by black solid lines) and its corresponding 95% CI (depicted by two red dashed lines) on the number of order statistics at depths 2, 3, $\cdots$ 10 for GOOG

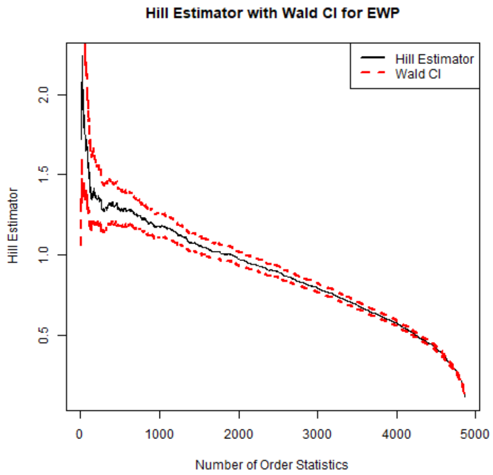

Figure 39: The dependence of estimated tail index α (represented by black solid line) and its corresponding 95% CI (depicted by two red dashed lines) on the number of order statistics for EWP for GOOG

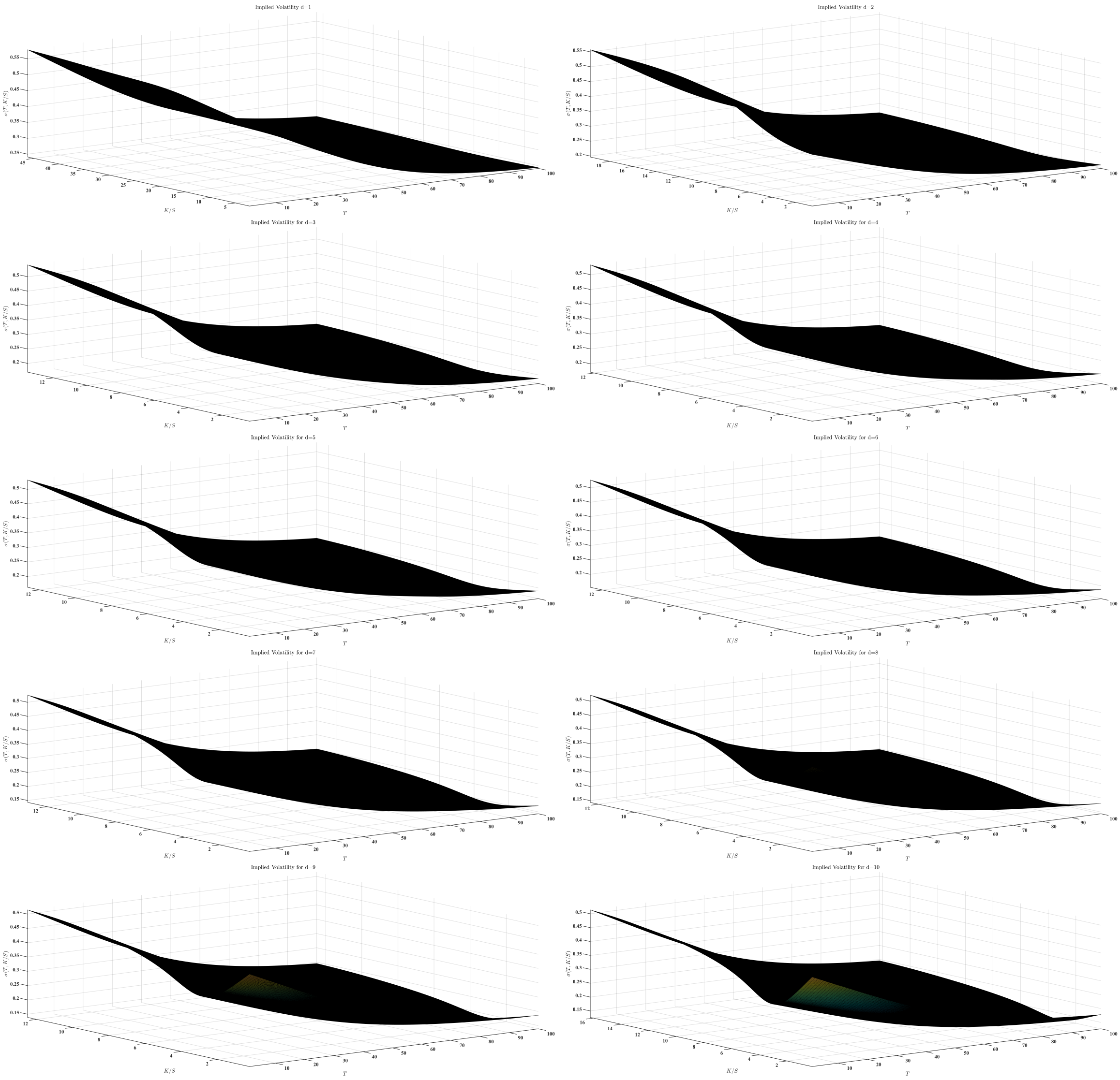

Figure 40: TMOBBAS Implied volatility surfaces for depths $1, 2, ..., 10$ for GOOG

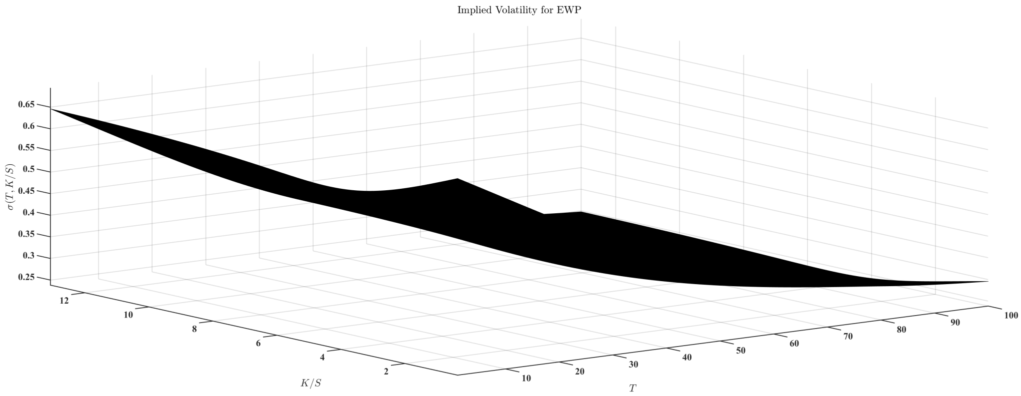

Figure 41: TMOBBAS Implied volatility surface for EWP

B.2.2 Figures for GMP

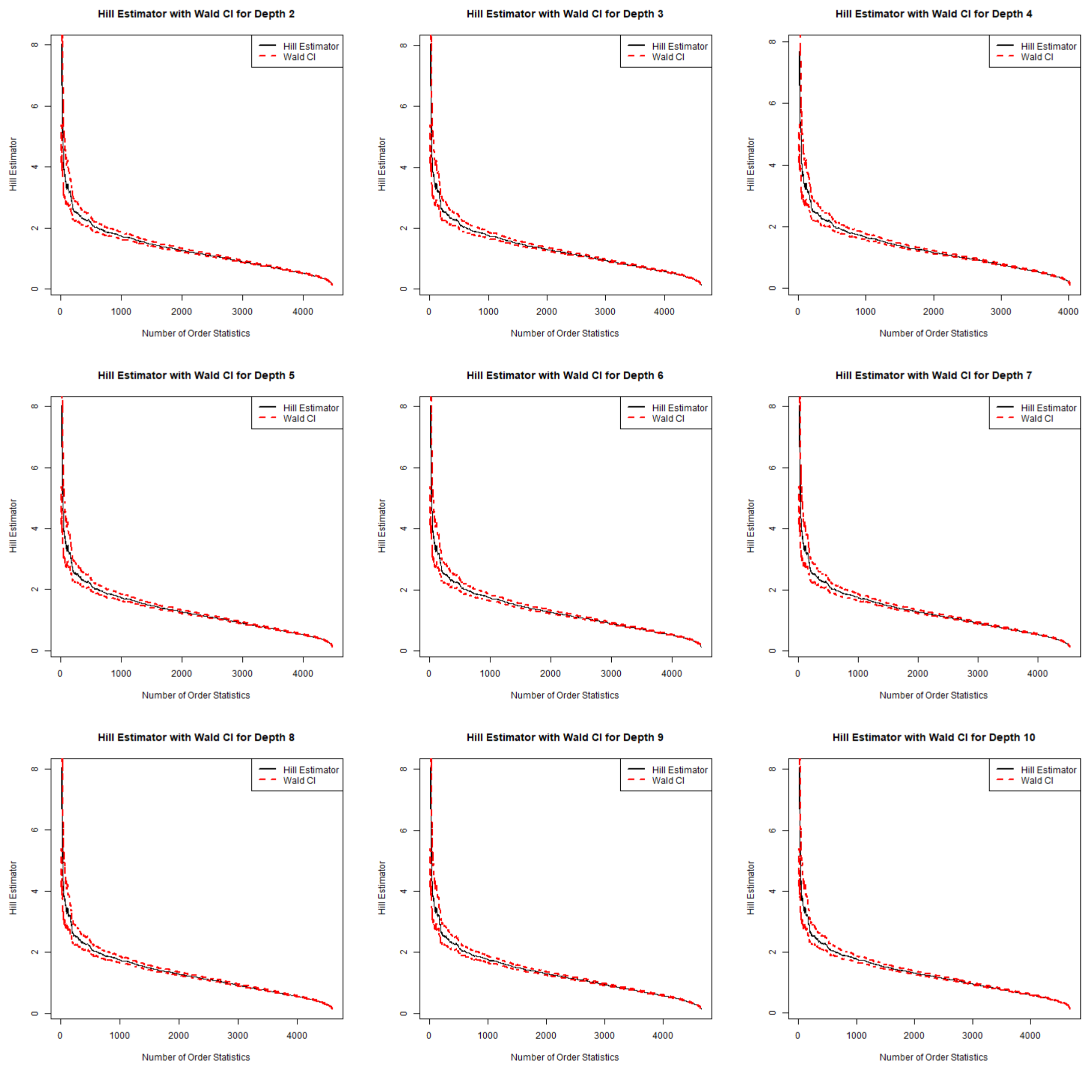

Figure 42: The dependence of estimated tail index α (represented by black solid lines) for GMP and its corresponding 95% CI (depicted by two red dashed lines) on the number of order statistics at depths 2, 3, $\cdots$ 10 for GOOG

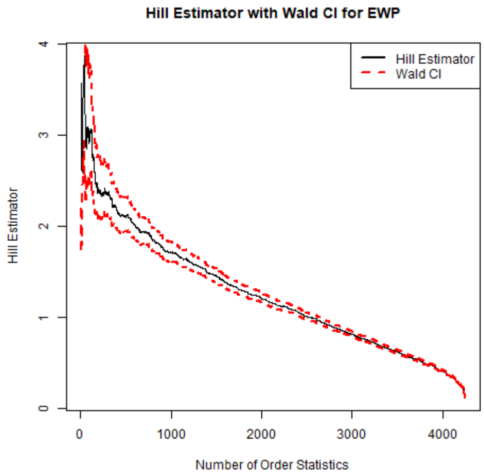

Figure 43: The dependence of estimated tail index α (represented by black solid line) of GMP and its corresponding 95% CI (depicted by two red dashed lines) on the number of order statistics for EWP for GOOG

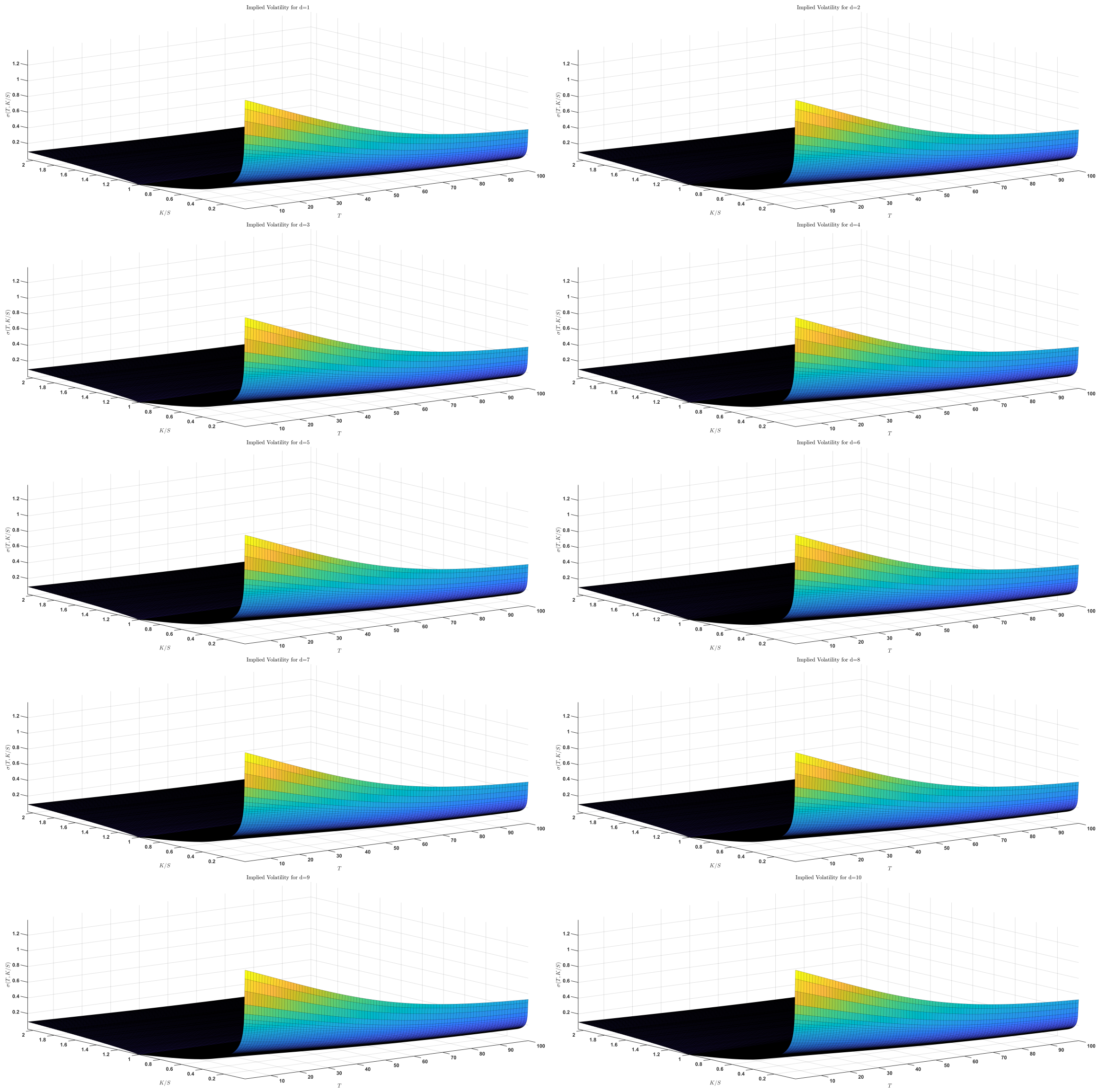

Figure 44: GMP Implied volatility surfaces for depths $1, 2, ..., 10$ for GOOG

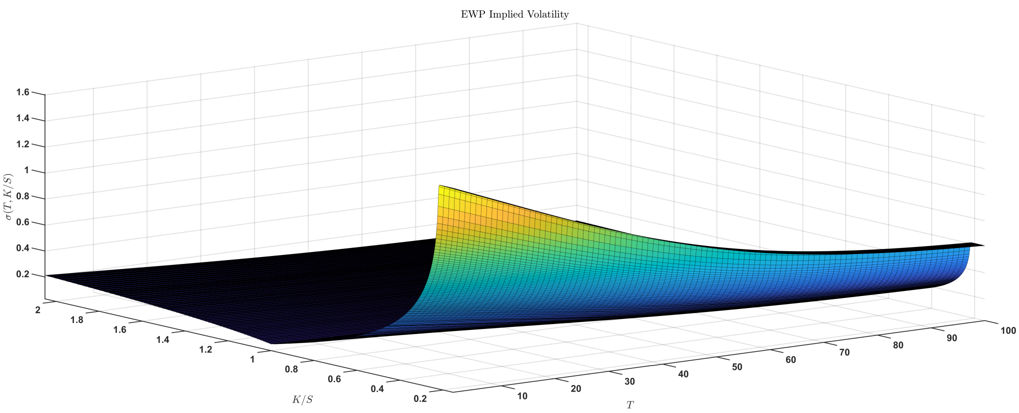

Figure 45: GMP Implied volatility surface for EWP